Chemical Science

ROYAL SOCIETY OF CHEMISTRY

EDGE ARTICLE

View Article Online
View Journal | View Issue



Cite this: *Chem. Sci.*, 2024, **15**, 11455

All publication charges for this article have been paid for by the Royal Society of Chemistry



# Multi-phosphine-chelated iron-carbide clusters *via* redox-promoted ligand exchange on an inert hexa-iron-carbide carbonyl cluster, $[Fe_6(\mu_6\text{-}C)(\mu_2\text{-}CO)_4(CO)_{12}]^{2-}$†

Caitlyn R. Cobb, Ren K. Ngo, Emily J. Dick, Vincent M. Lynch and Michael J. Rose *

We report the reactivity, structures and spectroscopic characterization of reactions of phosphine-based ligands (mono-, di- and tri-dentate) with iron-carbide carbonyl clusters. Historically, the archetype of this cluster class, namely $[Fe_6(\mu_6\text{-}C)(\mu_2\text{-}CO)_4(CO)_{12}]^{2-}$, can be prepared on a gram-scale but is resistant to simple ligand substitution reactions. This limitation has precluded the relevance of iron-carbide clusters relating to organometallics, catalysis and the nitrogenase active site cluster. Herein, we aimed to derive a simple and reliable method to accomplish CO → L (where L = phosphine or other general ligands) substitution reactions without harsh reagents or multi-step synthetic strategies. Ultimately, our goal was ligand-based chelation of an $Fe_n(\mu_n\text{-}C)$ core to achieve more synthetic control over multi-iron-carbide motifs relevant to the nitrogenase active site. We report that the key intermediate is the PSEPT-non-conforming cluster $[Fe_6(\mu_6\text{-}C)(CO)_{16}]$ (**2**: 84 electrons), which can be generated *in situ* by the outer-sphere oxidation of $[Fe_6(\mu_6\text{-}C)(CO)_{16}]^{2-}$ (**1**: *closo*, 86 electrons) with 2 equiv. of $[Fc]PF_6$. The reaction of **2** with excess $PPh_3$ generates a singly substituted neutral cluster $[Fe_5(\mu_5\text{-}C)(CO)_{14}PPh_3]$ (**4**), similar to the reported reactivity of the substitutionally active cluster $[Fe_5(\mu_5\text{-}C)(CO)_{15}]$ with monodentate phosphines (Cooke & Mays, 1990). In contrast, the reaction of **2** with flexible, bidentate phosphines (DPPE and DPPP) generates a wide range of unisolable products. However, the rigid bidentate phosphine bis(diphenylphosphino)benzene (bdpb) disproportionates the cluster into non-ligated $Fe_3$-carbide anions paired with a bdpb-supported Fe(II) cation, which co-crystallize in $[Fe_3(\mu_3\text{-}CH)(\mu_3\text{-}CO)(CO)_9]_2[Fe(MeCN)_2(bdpb)_2]$ (**6**). A successful reaction of **2** with the tripodal ligand Triphos generates the first multi-iron-chelated, authentic carbide cluster of the formula $[Fe_4(\mu_4\text{-}C)(\kappa3\text{-Triphos})(CO)_{10}]$ (**9**). DFT analysis of the key (oxidized) intermediate **2** suggests that its $(\mu_6\text{-}C)Fe_6$ framework remains fully intact but is distorted into an axially compressed, 'ruffled' octahedron distinct from the parent *closo* cluster **1**. Oxidation of the cluster in non-coordinating solvent allows for the isolation and crystallization of the CO-saturated, intact *closo*-analogue $[Fe_6(\mu_6\text{-}C)(CO)_{17}]$ (**3**), indicating that the intact $(\mu_6\text{-}C)Fe_6$ motif is retained during initial oxidation with $[Fc]PF_6$. Overall, we demonstrate that redox modulation beneficially 'bends' Wade-Mingo's rules *via* the generation of electron-starved (non-PSEPT) intermediates, which are the key intermediates in promoting facile CO → L substitution reactions in iron-carbide-carbonyl clusters.

Received 27th February 2024
Accepted 25th April 2024

DOI: 10.1039/d4sc01370k

rsc.li/chemical-science

## Introduction

The family of iron carbonyl carbide clusters well studied by Wampler *et al.*,[1] Churchill *et al.* 1971,[2] Churchill *et al.* 1974,[3] Beno *et al.*,[4] Tachikawa *et al.*,[5] and others was of substantial interest to organometallic chemists as models for Fischer–Tropsch chemistry and as a scaffold with highly fluxional ligands.[1–5] More recently, Berben *et al.* have investigated carbide and the closely related nitride clusters as small molecule catalysts for transformations like $CO_2$ reduction.[6–9] Since 2011, such carbide clusters have garnered attention from bioinorganic chemists as spectroscopic (and—aspirationally—structural or functional) models of the nitrogenase active site cluster (FeMoco) due to the authentic inorganic carbide that resides at the interstitial site.[10] However, attempts to transform these clusters into relevant FeMoco models *via* direct ligand substitution have met with limited success[11–13] and the presence of

*Department of Chemistry, The University of Texas at Austin, Austin, TX 78712, USA. E-mail: mrose@cm.utexas.edu*

† Electronic supplementary information (ESI) available. CCDC 2267255–2267260, 2267848, 2267849 and 2335756. For ESI and crystallographic data in CIF or other electronic format see DOI: https://doi.org/10.1039/d4sc01370k

ubiquitous CO ligands (and corresponding low, diamagnetic spin states) precludes their relevance to nitrogenase.

Historically, many of these clusters have proven a difficult platform upon which to achieve substitution of the CO ligands for anions—including biologically relevant sulfides, thiolates and alkoxides.[11,14] Some success has been reported, such as reactions of the six-iron cluster $[Fe_6(\mu_6\text{-}C)(\mu_2\text{-}CO)(CO)_{12}]^{2-}$ with strongly π accepting ligands such as $NO^+$ and $SO_2$ (and R–N≡C with nitride clusters).[15–17] Historically, the five-iron neutral cluster $Fe_5(\mu_5\text{-}C)(CO)_{15}$ was the first iron-carbide cluster (neé, metal-carbide cluster) to be isolated in 1962,[1] and its four-iron congener $Fe_4(\mu_4\text{-}C)(CO)_{13}$ was isolated several decades later (1981).[18] However, it has been decades since the ligand substitution reactions of neutral carbide clusters have been thoroughly explored. Notably, Cooke and Mays (1975) reported the reactivity of $Fe_5(\mu_5\text{-}C)(CO)_{15}$ with phosphines and showed that stronger σ donors ($PMe_2Ph$) resulted in a greater extent of substitution (1, 2 or 3 substitutions) than weaker σ donors ($PPh_3$, single substitution). To date, only one complex has been structurally characterized (Gourdon & Jeannin, 1990), namely $[Fe_5(\mu_5\text{-}C)(CO)_{11}(PMe_2Ph)_3]$.[19,20] Incidentally, the same report detailed the synthesis of a five-iron cluster ligated by bidentate phosphine bis(dimethylphosphine)ethane; however its X-ray structure was not disclosed.

Analogous substitution using $Fe_4(\mu_4\text{-}C)(CO)_{13}$ with $PR_3$ variants by Bradley resulted in preliminary structural data of thrice-substituted $[Fe_4(\mu_4\text{-}C)(\mu_3\text{-}CO)(CO)_9(PMe_3)_3]$, and a putative tetra-substituted variant was spectroscopically characterized by $^1H/^{13}C/^{31}P$ NMR.[21] Relatedly, a singly substituted phosphine variant was explored by Wadepohl, who reported the X-ray structure of the protonated four-iron cluster $[Fe_4(\mu_4\text{-}CH)(CO)_{12}(PPh_3)H]^-$;[22] this was an expansion on Muetterties' extensive body of work with the four-iron cluster series.[4,5,23]

The eventual aim of our research program is to systematically understand how to controllably insert a variety of multidentate ligands onto iron-carbide-carbonyl clusters pertaining to nitrogenase FeMoco. Indeed, the use of multidentate ligands to stabilize otherwise unisolable iron-sulfide clusters was a key milestone in Holm's foundational biomimetic work with $Fe_3S_4$-type clusters.[24–26] Recent successes achieved by Suess and coworkers include the isolation of previously unisolable FeS clusters with extended multidentate ligand scaffolds; this includes their isolation of an elusive alkyl-$[Fe_4S_4]^{3+}$ cluster stabilized by a scorpionate ligand.[27] A report by Agapie *et al.* employing a multidentate bis(diisopropylamino)cyclopropenylidene (BAC) ligand to give a carbyne FeS cluster is also notable.[28,29] This approach has yet to be applied to iron clusters that contain the authentic inorganic carbide, in large part due to the challenges in controlling CO substitution (and prevention of cluster disproportionation) as discussed above. Instead, some of the most biologically relevant models to date have approached FeMoco models with a 'carbide-like' motif bound to iron centers.[30,31] We sought in this work to elucidate the design principles and ligand-binding preferences of iron-carbide-carbonyl clusters with commercially available, multidentate phosphine ligands as a stepping stone towards more biomimetic chemistry. We hypothesized that such phosphine ligands would accelerate our understanding of intra-cluster (preferred) *vs.* inter-cluster (not preferred) binding, apical *vs.* equatorial ligation, and 'single-site chelation' *vs.* 'multi-site chelation' preferences. We deemed phosphine substitution onto substitutionally active, neutral clusters like $Fe_5(\mu_5\text{-}C)(CO)_{15}$ as the preferred route to design stable chelation modes.

The primary synthetic obstacle to performing such reactions is the need to isolate the neutral $Fe_5(\mu_5\text{-}C)(CO)_{15}$ cluster,[32] whose low yield in our hand (5–15%) from gram-scale quantities of $[Fe_6(\mu_6\text{-}C)(CO)_{16}]^{2-}$ severely limited the scope and depth of explorative chemistry. In related work, Zacchini *et al.* reported the redox-enabled addition of Lewis acids, utilizing the two-electron reduction of $[Fe_6(\mu_6\text{-}C)(CO)_{16}]^{2-}$ to $[Fe_6(\mu_6\text{-}C)(CO)_{15}]^{4-}$ (structurally characterized), which then stably binds $Au(PPh_3)^+$ and $H^+$ without cluster disproportionation.[33] Notably, both anionic precursors conform to the polyhedral skeletal electron pair theory (PSEPT) electron counting regime, wherein both clusters possess 84 $e^-$ in accordance with the $14n + 2$ rule for *closo* structures. Thus, the synthetic addition of Lewis acid 'ligands' like $H^+$ or $Au(PPh_3)^+$ does not violate PSEPT.

In contrast to the addition of Lewis acids enabled by *reduction*, we wished to pursue the addition of Lewis bases enabled by *oxidation*. As such, we envisioned that the two-electron oxidation of $[Fe_6(\mu_6\text{-}C)(CO)_{16}]^{2-}$ to the non-PSEPT intermediate $[Fe_6(\mu_6\text{-}C)(CO)_{16}]$ (82 $e^-$; 2 $e^-$ short of PSEPT rules) would facilitate the addition of 2 $e^-$ ligand(s) such as phosphine. This strategy builds on our previous work, wherein we reported that the addition of two CO ligands to $[Fe_6(\mu_6\text{-}C)(CO)_{16}]$ (82 $e^-$) afforded the isolable *nido* species $Fe_6(\mu_6\text{-}C)(CO)_{18}$ (88 $e^-$, $14n + 4$).[32] In this work, we utilize the *in situ* oxidation of $[Fe_6(\mu_6\text{-}C)(CO)_{16}]^{2-}$ to promote binding of phosphine-based ligands without proceeding through the low-yielding $Fe_5(\mu_5\text{-}C)(CO)_{15}$ or $Fe_4(\mu_4\text{-}C)(CO)_{13}$ clusters. We demonstrate the benefits of this synthetic route and report the structures and spectroscopic properties of novel (authentic) carbide clusters supported by multidentate phosphines that drive towards the lower CO/Fe ratios, which are ultimately necessary for biological relevance to nitrogenase active sites.

## Results and discussion

### Redox activation for ligand substitution and isolation of *closo*-$Fe_6(\mu_6\text{-}C)(CO)_{17}$ (3)

In 1971, Churchill predicted the isolability of a neutral 86 $e^-$ cluster of the formula *closo*-$Fe_6(\mu_6\text{-}C)(CO)_{17}$.[2,3] In a 2017 report, we isolated the closely related, neutral 88 $e^-$ species *nido*-$Fe_6(\mu_6\text{-}C)(CO)_{18}$, whose formulation was justified on the basis of (i) strong Raman features indicative of highly symmetric breathing modes (corroborated by DFT calculations); (ii) the lack of bridging CO features in the IR spectrum; (iii) a Mössbauer spectrum indicating the presence of 'three pairs' of equivalent iron centers.[32] Thus, the possibility of the long-predicted 86 $e^-$ species *closo*-$Fe_6(\mu_6\text{-}C)(CO)_{17}$—incidentally, whose Ru-based congener is structurally characterized[34]—was excluded by the above evidence. Synthetically, 88 $e^-$ *nido*-$Fe_6C(CO)_{18}$ was isolated *via* outer-sphere oxidation of the 86 $e^-$ cluster of the formula *closo*-$[Fe_6C(CO)_{16}]^{2-}$ (**1**) in tetrahydrofuran (THF) under

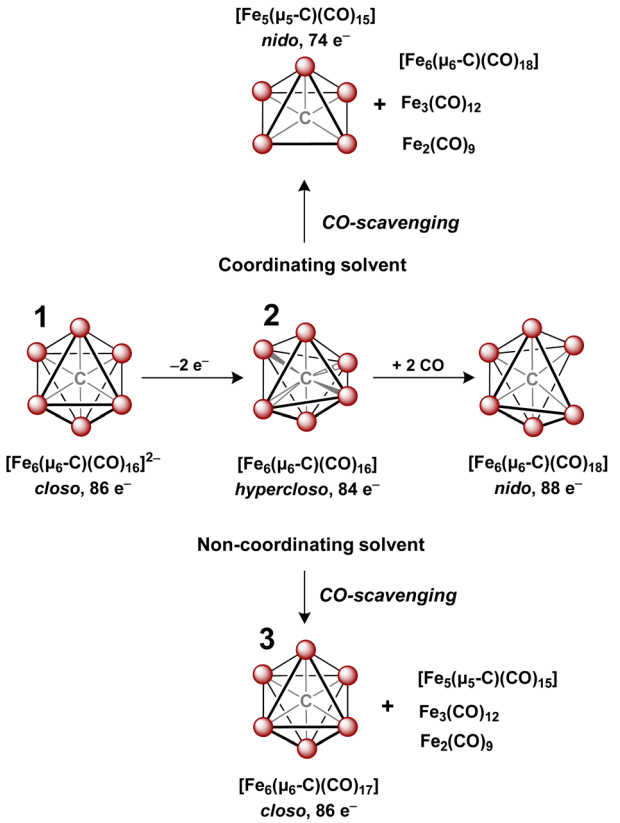


Scheme 1 Oxidation of **1** (center left) to form the key hypercloso intermediate **2**, (center). The subsequent reaction with the CO atmosphere forms an intact and isolable *nido* cluster (center right). Without CO, it forms the two disproportionate families of iron(carbide) carbonyls shown at top and bottom in coordinating and non-coordinating solvents, respectively. The intact and isolable cluster **3** is only formed and stable in non-coordinating solvent, unlike all the other clusters shown.

a CO atmosphere.[32] DFT calculations accurately predicted the *nido* configuration of $Fe_6(\mu_6\text{-}C)(CO)_{18}$ in the form of an open-faced, pentagonal neutral cluster—consistent with the PSEPT $14n + 4$ rule for *nido* clusters. In the absence of a CO atmosphere, the oxidation of **1** in THF ultimately results in cluster decay, as the cluster scavenges carbonyls from itself, disproportionating to a mixture of neutral products including $Fe_6(\mu_6\text{-}C)(CO)_{18}$, $Fe_5(\mu_5\text{-}C)(CO)_{15}$ and $Fe_3(CO)_{12}$, upon both 1 and 2 $e^-$ oxidation.[32,35] We thus hypothesized that an *in situ*,

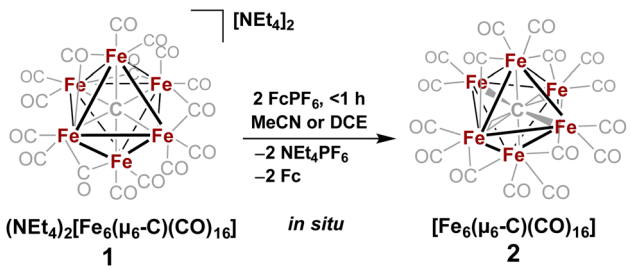


Scheme 2 *In situ* oxidation of **1** to form the non-PSEPT intermediate **2**, the key precursor to all of the ligand additions in this report.

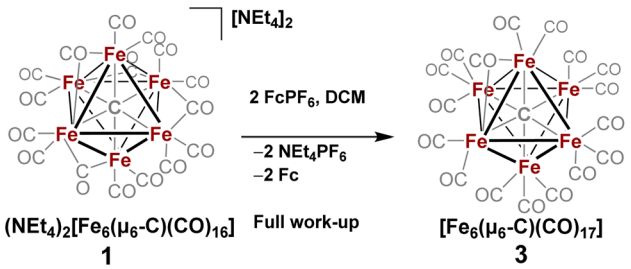


Scheme 3 *In situ* oxidation of **1** in non-coordinating solvent to form **3**, the stable six-iron *closo* cluster.

outer-sphere oxidation of cluster **1** would generate a *metastable*, non-PSEPT cluster—putatively the 84 $e^-$ cluster $[Fe_6(\mu_6\text{-}C)(CO)_{16}]$ (**2**) (*vide infra* for computational details). Due to its under-coordination (*i.e.* low PSEPT $e^-$ count), we posited that this cluster would have a high affinity for the addition of exogenous ligands (Schemes 1–3).

The validity of the above approach was tested by the reaction of a deep violet MeCN solution of **1** with 2.1 equiv. of $[Fc]PF_6$ to generate cluster **2**. The IR spectrum was monitored, and over the course of 30 min the terminal CO features [1892(s), 1925(s) and 2032(w) $cm^{-1}$] and the bridging CO feature [1760(m) $cm^{-1}$] were diminished in intensity. The reddened solution exhibited a blue-shifted set of terminal CO features at 1963(s), 1985(s), 2036(w) and 2087(w) $cm^{-1}$—indicative of cluster oxidation (Fig. 1). The IR spectrum was persistent for several hours, but at extended times (12–24 h, in the dark) the CO features broadened, indicative of cluster disproportionation and/or decay.

However, when this reaction was conducted in non-coordinating DCM, significant differences were observed. Upon addition of 2.5 equiv. of $[Fc]PF_6$ to a violet DCM solution of **1** the solution turned black. After 10 minutes, the solvent was removed *in vacuo* and washed with pentane, diethyl ether

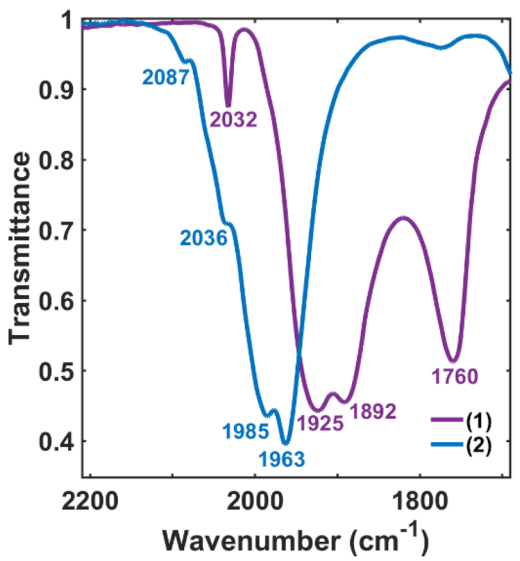


Fig. 1 IR spectra of drop-cast samples during the oxidation of **1** (violet) to form **2** (blue) in MeCN.

($Et_2O$), and toluene to remove ferrocene and $Fe_5(\mu_5\text{-}C)(CO)_{15}$. Extraction into fluorobenzene (FPh) resulted in a deep black solution, which upon cooling afforded diffraction-quality black prisms of the long predicted *closo*-$Fe_6(\mu_6\text{-}C)(CO)_{17}$ (**3**). We drew from this unexpected result the following conclusions: first, the initial oxidized intermediate **2** is an intact, six-iron species; second, the *closo* neutral species **3** is unstable in coordinating solvents such as THF and MeCN and likely decomposes into $Fe_6(\mu_6\text{-}C)(CO)_{18}$, $Fe_5(\mu_5\text{-}C)(CO)_{15}$ and $Fe_3(CO)_{12}$, leading to its reddish color; third, as observed in the 2017 report, excess $CO_{(g)}$ is required as the ligand to prevent the disproportionation of product six-iron clusters due to the instability of **2**. On this basis, we selected a <1 h timeframe for *in situ* ligand addition and moving forward the solvent choice in each reaction.

### Reaction of 2 with monodentate phosphines: dimethylphenylphosphine ($PMe_2Ph$) and $PPh_3$

The only phosphine-substituted, iron-carbide-carbonyl cluster reported in the CSD is that of Gourdon & Jeannin, namely $Fe_5(\mu_5\text{-}C)(CO)_{12}(PMe_2Ph)_3$, which was prepared in a straightforward fashion from $Fe_5(\mu_5\text{-}C)(CO)_{15}$ and $PMe_2Ph$.‡ [20] On this basis, $PMe_2Ph$ was selected to validate the proposed synthetic approach. The addition of ~9 equiv. of $PMe_2Ph$ to *in situ*-generated **2** in DCE red-shifted the most intense $\nu$(CO) feature from 1990 → 1950 $cm^{-1}$, consistent with $PMe_2Ph$ binding.[20] Further spectroscopic evidence for $PMe_2Ph$ binding was observed following column chromatography: The triply substituted cluster $[Fe_5(\mu5\text{-}C)(CO)_{12}(PMe_2Ph)_3]$ was identified by its characteristic IR features (2045, 1928, and 1857 $cm^{-1}$) and $^{31}P$ NMR resonances ($CDCl_3$: $\delta$ 18.4, 22.1 ppm).[20] However, this species proved unisolable due to the presence of other putative species such as doubly substituted $Fe_5(\mu_5\text{-}C)(CO)_{13}(PMe_2Ph)_2$ and singly substituted $Fe_5(\mu_5\text{-}C)(CO)_{14}(PMe_2Ph)$. Nonetheless, these IR data overall provided strong evidence that the *in situ*-oxidized species **2** (six-iron cluster) provided an analogous pattern of ligand substitution to the five-iron cluster $Fe_5(\mu_5\text{-}C)(CO)_{15}$.

To minimize the number of substitution products, we reasoned that a weaker phosphine ligand like $PPh_3$ would provide a more tractable cluster—despite the lack of crystallographic precedent.[19] According to Cooke & Mays, the reaction of 9 equiv. of $PPh_3$ with *in situ*-generated **2**—followed by

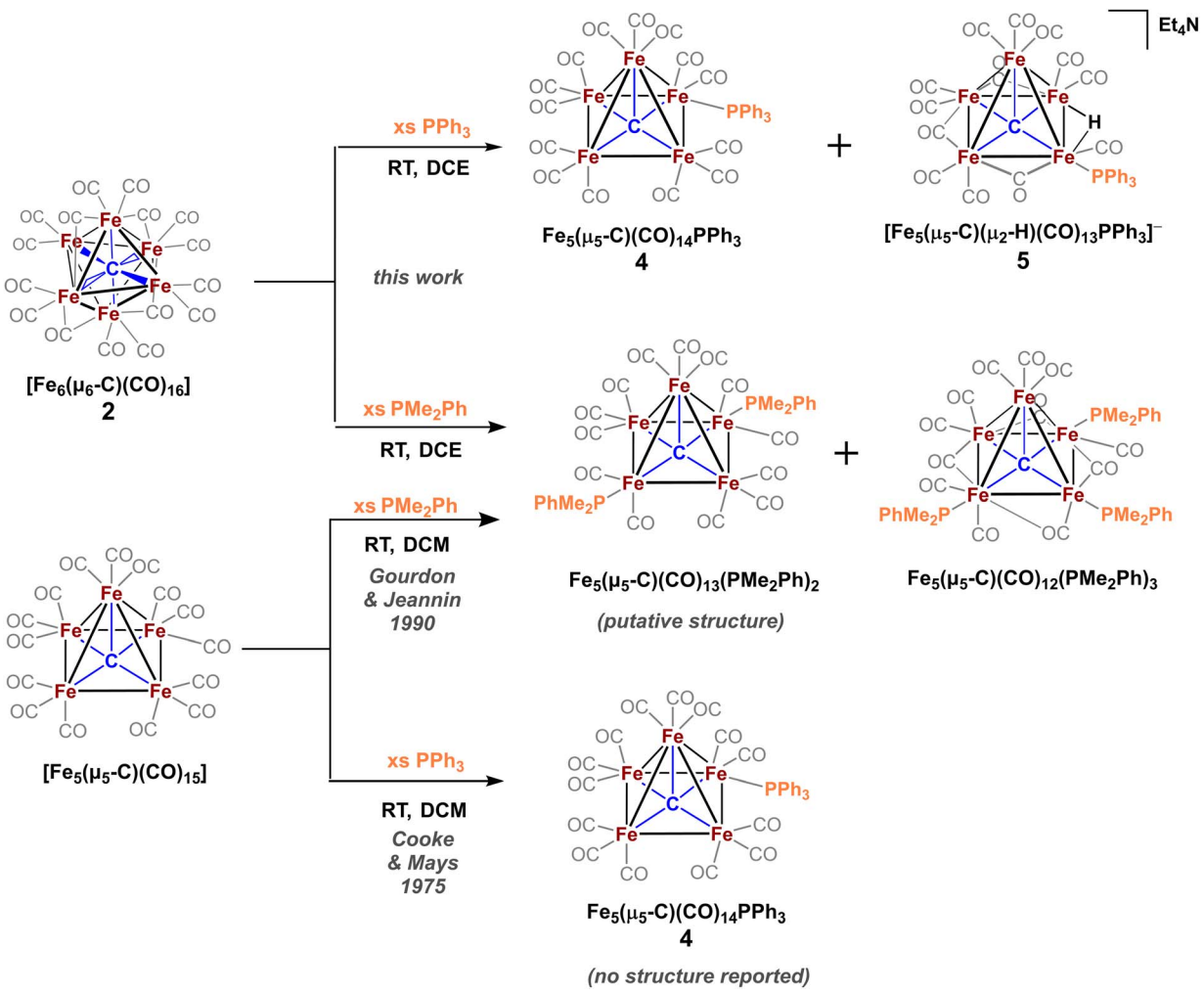


Scheme 4 Reactions of the neutral, six-iron (top) and five-iron (bottom) clusters with the monodentate phosphines $PMe_2Ph$ and $PPh_3$ to form singly, doubly, and triply bound phosphine supported five-iron clusters.

differential extraction ($Et_2O$ *vs.* FPh) and air-free chromatography—provided two modified clusters: black plates of $Fe_5(\mu_5\text{-}C)(CO)_{14}(PPh_3)$ (**4**, reported but not crystallized by Cooke & Mays), and red-violet plates of the novel hydride species $NEt_4[Fe_5(\mu_5\text{-}C)(\mu_2\text{-}H)(\mu_2\text{-}CO)_3(CO)_9(PPh_3)]$ (**5**, Scheme 4). Notably, the hydride cluster **5** was not identified in the spectroscopic analyses performed by Cooke & Mays (IR, $^{31}P$ NMR, and EA).[19]

Additional observations shed light on the stoichiometry and variance in product profiles between our work using the six-iron cluster **2**, *versus* Cooke & Mays using the five-iron cluster $Fe_5(\mu_5\text{-}C)(CO)_{15}$. The initial extraction of the $PPh_3$ reaction mixture with pentane ultimately provided (in addition to copious amounts of ferrocene) chiffon-coloured blocks of the non-carbide complex $Fe(CO)_4(PPh_3)$. The isolation of such a mononuclear iron species provides insight into the stoichiometric decapping reaction that must occur in the conversion of six-iron clusters to five-iron clusters. That is, the loss of one iron in the transformation of **2** to **4** is accounted for by the formation of $Fe(CO)_4(PPh_3)$. However, the origin of the anionic hydride species **5** was not explained. We speculate that the zero-valent iron present in $Fe(CO)_4(PPh_3)$ could act as a reductant—thus forming $[Fe^n(CO)_x(PPh_3)_y](PF_6)_n$, where $n = 1$, 2—in the formation of the anionic hydride species **5**.[36]

### Reaction of 2 with bidentate phosphines: dppe, dppp and bdpb

To explore phosphine substitution more controllably, bidentate phosphines were utilized to leverage the chelate effect. The reactions of *in situ*-generated **2** in DCE with two equiv. of dppe or dppp provided a multitude of carbonyl-containing products (over 15)—most of which were unisolable (despite varying solvent extractions and chromatography), and some of which were isolable but not amenable to crystallization.

We next selected a rigid bisphosphine, namely 1,2-bis(diphenylphosphino)benzene (bdpb). Intriguingly, the reaction of two equiv. of bdpb with **2** in MeCN afforded no isolable, phosphine-bound clusters. Instead, red plates of the 'compound' iron species $[Fe_3(\mu_3\text{-}CH)(CO)_{10}]_2[Fe^{II}(MeCN)_2(bdpb)_2]$ (**6**, Scheme 5) were isolated from $Et_2O$. The observation of this low nuclearity three-iron $\mu_3$-CH species indicates a greater extent of cluster deconstruction *via* iron 'clipping' by the chelating ligands. This is in contrast to the intact iron-carbide-phosphine clusters obtained using the monodentate phosphines ($PPh_3$ and $PMe_2Ph$).

Ultimately, we attribute the lack of success in the bidentate approach to two factors. First, the inherent flexibility of the ethyl or propyl linkers, which contributes to the intractability of the product profile and difficulty in crystallizing products. Second, there are two sub-factors that preclude the desired 'edge' chelation on an intact cluster: (i) the limited span of the ethyl or propyl linkers in dppe and dppp and (ii) the constrained geometry of bdpb, which absolutely enforces single-site chelation. Indeed, the isolation of compound **6** illustrates that enforced, single-site chelation leads merely to lower nuclearity, unsubstituted clusters (alongside mono-iron products).

Some comparative insight is gained by inspection of the analogous ruthenium-carbide literature: Webster *et al.* elegantly demonstrated that the carbon chain length in a bis(diphenylphosphine) series (1–4 $CH_2$ units: dppm, dppe, dppp, and dppb, respectively) were crystallographically or spectroscopically demonstrated to determine the chelation mode on $Ru_5$ clusters. For example, dppm and dppe only exhibit binding at a single Ru site; in contrast, dppp binds at two adjacent Ru vertices. Furthermore, the longest carbon chain in dppb facilitates binding of the $Ru_5$ cluster at opposite vertices.[37] Such isolable Ru clusters exhibit greater kinetic stability than the corresponding Fe clusters and thus may provide 'snapshots' of the unisolable Fe clusters that might enable the reactions presented herein.

### Reaction of 2 with tridentate phosphines

We reasoned that alkyl-linked bis-phosphines (*vide supra*) had a similar propensity to extract single, chelated iron sites from carbide-based clusters (per bdpb, cluster **6**). On this basis, we first selected the linear tridentate phosphine ligand bis(2-diphenylphosphinoethyl)phenylphosphine (Scheme 6). However, the reaction of 1.1 equiv. of $(Ph_2PCH_2CH_2)_2PPh$ with **2** led to only one isolable product. Extraction with toluene followed by chromatography and pentane vapor diffusion afforded the three-iron cluster **7**, which exhibits a pseudo-$(\mu_3\text{-}C)Fe_3$ core supported by 8 CO ligands and the multi-dentate phosphine ligand (Scheme 6). Notably, **7** exhibits one desirable property and one undesirable property: The desirable property is successful bidentate chelation of a single iron site, which remains bound to the 'carbide' core. The undesirable property is that the third phosphine is covalently bonded to the central carbon; notably, the $R_3P\text{–}C(\mu_3)Fe_n$ motif is reminiscent of the heterometallic cluster $[(\mu_3\text{-}CPMe_3)(Fe(CO)_3)_2Co(CO)_3]^-$ reported

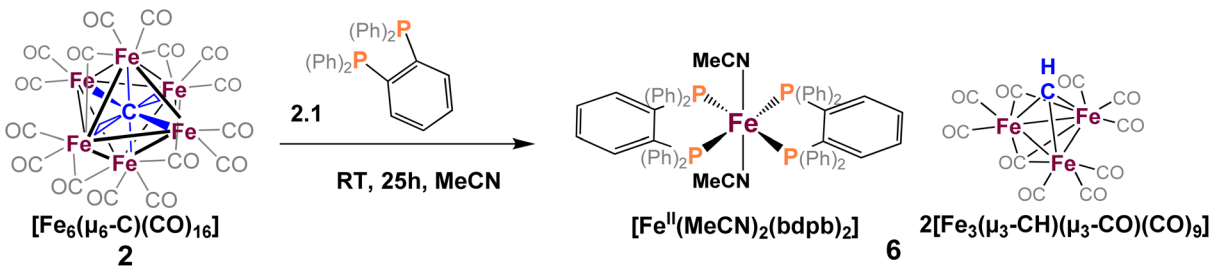


Scheme 5 Reaction of 1,2-bis(diphenylphosphino)benzene (bdpb) with **2**, $[Fe_3(\mu_3\text{-}CH)(CO)_{10}]_2[Fe^{II}(MeCN)_2(bdpb)_2]$ co-crystallized as **6**.

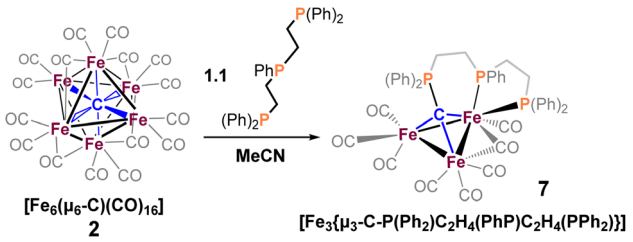


Scheme 6 Reaction of $(Ph_2PCH_2CH_2)_2PPh$ with **2**, generating $[Fe_3(\mu_3\text{-}C\text{-}P(Ph_2)C_2H_4(PhP)C_2H_4(PPh_2))]$ (**6**).

by Shriver.[38] Ultimately, the formation of the P–C bond diverged from our goal of retaining the authentic inorganic carbide.

We thus speculated that the third phosphine could not extend all the way to the adjacent iron site. As such, we considered the longer propyl-linked congener $(Ph_2PCH_2CH_2CH_2)_2PPh$, but this ligand is not commercially available. An intriguing alternative was the commercially available (tripodal) ligand Triphos, which utilizes 3-carbon linkers between each phosphine in a tripod rather than a linear format. The reaction of **2** with two equiv. Triphos in DCE provided fewer products than the 'linear' triphosphine, and most of these products proved crystallographically tractable. Indeed, several Triphos-ligated iron clusters were ultimately isolated from this reaction: pentane extraction provided ferrocene, unreacted Triphos, and two distinct black iron-carbonyl products. The first product exhibited strongly blue-shifted $\nu_{CO}$ features [2077 (m), 2022(s), and 2006 $cm^{-1}$ (s)] and no bridging CO features. The crystallization of this species afforded grey-green needles of $Fe_5(\mu_5\text{-}C)(CO)_{14}(\kappa_1\text{-Triphos})$ (**8**), wherein one Triphos 'arm' displaces a single CO on an otherwise unperturbed five-iron framework (Scheme 7, Fig. 5).

The second product was minimally soluble in pentane, but it was ultimately isolated in greater quantities *via* $Et_2O$ extraction. Column purification provided green-black crystals of the desired, $\kappa_3$-Triphos cluster $Fe_4(\mu_4\text{-}C)(\mu_2\text{-}CO)(CO)_8(\kappa_3\text{-Triphos})$ (**9**). This cluster represents the first multi-iron chelated iron-carbide cluster, and its structural metrics and implications are discussed further below (*vide infra*, X-ray section). The subsequent red band (THF eluent; vapor diffusion of hexane into toluene) provided deep red prisms identified as the 'clipped' cluster $Fe_3(CO)(CO_2)Fe(CO)(\kappa_3\text{-Triphos})$ (**10**). This cluster exhibits a distal $\{(\kappa_3\text{-Triphos})Fe(CO)\}^{2+}$ moiety linked to the $Fe_3$ core by a $\{\mu_3\text{-}CCO_2\}^{4-}$ bridge. The formation of both **10** and **9** (four-iron clusters) from **8** (five-iron cluster) as the common precursor was confirmed by dissolution of **8** in MeCN (Scheme 7), which then provided clusters **9** and **10** as the primary products.

Notably, both the 'clipped' **10** and 'intact' **9** comprise four irons; we thus postulated **9** as the precursor to **10**. However, the dissolution of **9** in toluene followed by crystallization provided evidence against this hypothesis: Crystallographic analysis of the resulting black crystals revealed a phenyl transfer reaction from a $PPh_2$ moiety to the carbide, thus forming a $(\mu_3\text{-}CPh)Fe_3$ core in **11**. In parallel, re-crystallization attempts of **9** in $Et_2O$ lead to isolation of the (known) mononuclear species $(Triphos)Fe(CO)_2$, whose formation stoichiometrically accounts for the loss of one iron site in the conversions **2** → **8**, **8** → **9** and **9** → **11**.

We suspected cluster **8** (with the $\kappa_1$-Triphos motif) to be a precursor to the more highly substituted clusters **9** and **10**. To explore this hypothesis, the addition of MeCN to a light hazel solution of **8** in $Et_2O$ induced an immediate color change to amber. After 3 min, the IR spectrum no longer exhibited the $\nu_{CO}$ features of **8** (2079 $cm^{-1}$), and a very broad and red-shifted feature near 1980 $cm^{-1}$ was observed (Fig. S36†). Ultimately

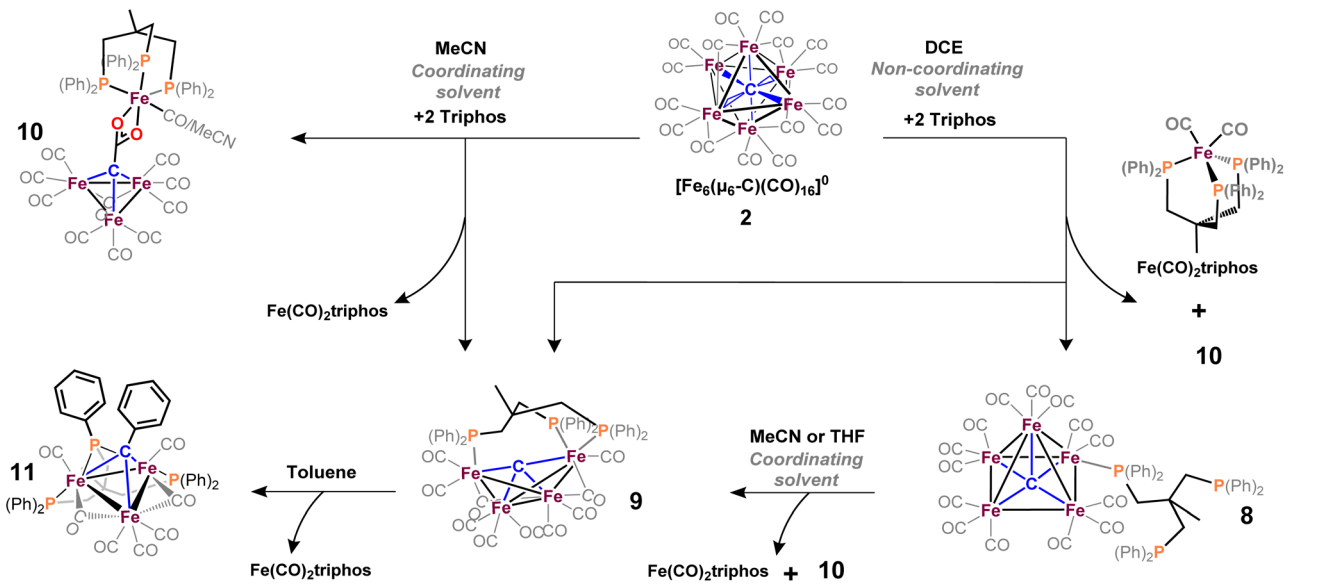


Scheme 7 Reactions of **2** with tripodal Triphos in MeCN (left) and non-coordinating DCE (right). The reaction in DCE forms complexes **8**, **9**, and **10** and monometallic $Fe(CO)_2$Triphos. The reaction of **2** with Triphos in MeCN affords the same reaction products except **8**. The addition of MeCN or THF to **8** ultimately does provide compounds **9**, **10** and $Fe(CO)_2$Triphos. The extended decomposition reaction of **9** in non-coordinating solvent affords **11**.

chromatographic, IR and X-ray analyses revealed the presence of **9** and **10**. This unambiguously demonstrates the solvent-induced (MeCN) cluster conversion of **8** → **9** + **10**. The same result was obtained in THF (albeit over hours, not seconds), suggesting the accelerative role of coordinating solvent to facilitate complete Triphos coordination (*i.e.* CO displacement) onto these clusters.

### X-ray structures

**$Fe_6(\mu_6\text{-}C)(CO)_{17}$ (3).** The structure of the neutral, *closo* species **3** is consistent with the 17 carbonyl analogue of the Ru cluster $Ru_6(\mu_6\text{-}C)(CO)_{17}$ first reported by Johnson *et al.* in 1967.[34] Both clusters maximize symmetry with a single bridging carbonyl and sixteen terminal carbonyls giving each iron three coordination sites. Cluster **3** crystallizes with two separate 'half clusters' per unit cell, shown in Fig. 2 as a grown structure with two intact clusters. The Fe–C distances are consistent, all between 1.889 and 1.914 with only a 0.01 difference between axial and equatorial sites. These bond lengths are comparable, albeit slightly longer than those in the dianionic *closo* compound **1** (see Table 5) and range from 1.874(5) to 1.898(5). Overall, it embodies exactly the predictions for a *closo*, neutral six-iron carbide cluster, with no deviations from other known six-iron *closo* compounds.

**$Fe_5(\mu_5\text{-}C)(CO)_{14}(PPh_3)$ (4).** The substitution of one $PPh_3$ onto the five-iron framework (Fig. 3, left) is consistent with the formula assigned by Cooke & Mays based on IR, NMR and elemental analysis.[19] Cluster **4** is the first structurally characterized $Fe_5$-carbide cluster with a single phosphine bound to the framework. The location of $PPh_3$ at a basal Fe site (as opposed to the apical site) is consistent with the regioselectivity reported in Gourdon & Jeannin's X-ray structure of the tri-substituted cluster $Fe_5(\mu_5\text{-}C)(CO)_{12}(PMe_2Ph)_3$ and with the corresponding isoelectronic $Fe_5$-nitride/phosphine cluster $[Fe_5(\mu_5\text{-}N)(CO)_{13}(PPh_3)]^-$ reported by Berben.[7,20]

In the basal $Fe_4$ plane, the $(PPh_3)Fe_1$–$Fe_2$ and $(PPh_3)Fe_1$–$Fe_4$ bond distances are 2.7362(15) and 2.6998(15) Å, respectively. These distances are longer than the athwart $Fe_3$–$Fe_2$ and $Fe_3$–$Fe_4$ distances [2.6341(16) and 2.6326(16) Å]. We attribute the longer $Fe_1$-based distances to a more electropositive $Fe_1$ site (*versus* $Fe_3$). We posit that this is a result of the stronger $PPh_3$ σ donation to $Fe_1$, and the compensatory electron density at the $Fe_3(CO)_3$ moiety, which has greater $Fe(d_\pi)|CO(\pi^*)$ back-bonding. The basal plane iron carbide exhibits only a slight elongation of the $Fe_3$–$C_1$ bond [the iron site diagonal to phosphine binding: $Fe_1$–$C_1$ 1.888(8) Å and $Fe_3$–$C_1$ 1.932(8) Å] (Table 1). The carbide C–$Fe_5$(apical) bond [1.949(8) Å] is nearly identical to that found in the unsubstituted parent cluster $Fe_5(\mu_5\text{-}C)(CO)_{15}$, namely 1.948(7) Å. However, the displacement of the carbide from the basal plane (see the visualization in Fig. S47†) in **4** [$d = 0.145$ Å] is greater than the displacement found in the parent cluster [$d = 0.09$ Å]. This is consistent with the previously observed trend of increased carbide displacement with increased cluster electron density.[20,39] For example, both the dianion $[Fe_5(\mu_5\text{-}C)\mu_2\text{-}(CO)_2(CO)_{12}]^{2-}$ and the triply substituted cluster $Fe_5(\mu_5\text{-}C)(CO)_{12}(PMe_2Ph)_3$ exhibit greater carbide displacements [0.18 and 0.20(1) Å, respectively] than the parent neutral cluster.[20,32]

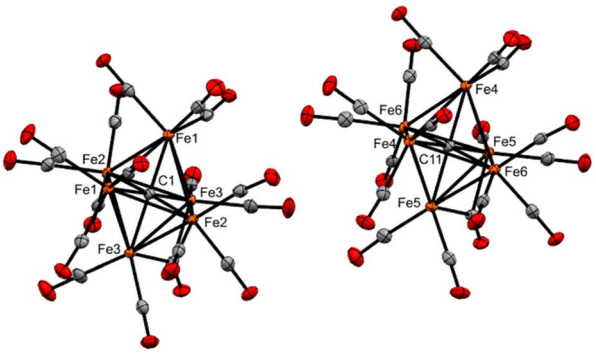


Fig. 2 ORTEP diagram (50% thermal ellipsoids) for $Fe_6(\mu_6\text{-}C)(CO)_{17}$ (**3**), shown as a grown structure of an asymmetric unit cell with two half-clusters (see ESI, Fig. S37†).

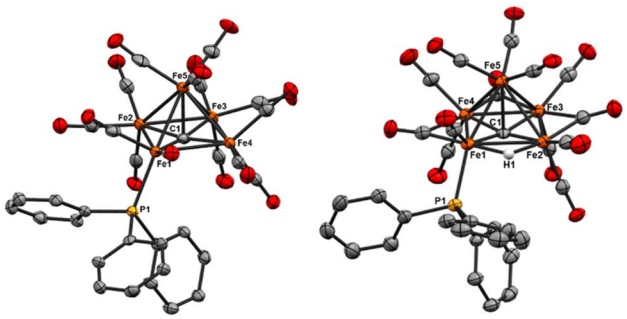


Fig. 3 ORTEP diagram (50% thermal ellipsoids) for the mono-substituted $Fe_5$ clusters $Fe_5(\mu_5\text{-}C)(CO)_{14}PPh_3$ (**4**, left) and the anion of $NEt_4[Fe_5(\mu_5\text{-}C)(\mu_2\text{-}H)(CO)_{13}PPh_3]$ (**5**, right); H atoms are omitted for the sake of clarity except for the hydride in **5**. The $NEt_4$ cation is omitted from **5** for the sake of clarity.

**$NEt_4[Fe_5(\mu_5\text{-}C)(\mu_2\text{-}H)(CO)_{13}PPh_3]$ (5).** To our knowledge, **5** (Fig. 3, right) represents the first reported five-iron, hydride-carbide carbonyl cluster. Our initial formulation of **5** based on diffraction data was the non-hydride cluster $NEt_4[Fe_5(\mu_5\text{-}C)(\mu\text{-}CO)_3(CO)_{10}PPh_3]$; this was perplexing, as the putative odd-electron count (73 $e^-$) and non-PSEPT conformity were unprecedented. However, our initial spectroscopic analysis ($^{31}P$ NMR: 62.17 ppm; EPR: no identifiable signal) of **5** contra-indicated the putative 73 $e^-$ count. Closer inspection of the bridging carbonyl motifs revealed that three out of the four basal edges hosted a μ-CO unit, while the fourth edge presented an apparent 'open' binding site. We thus reasoned that a hydride ligand might occupy this open site, which would provide a diamagnetic 74 $e^-$ count (PSEPT $14n + 4$, *nido*) consistent with the above spectroscopic observations. Upon re-investigation of the X-ray data, the inclusion of a $\mu_2$-H motif improved the *R* value from 5.31% to 4.60%. Furthermore, the extension of $^1H$ NMR analysis into the upfield hydride region revealed a resonance at −11.5 ppm, and this resonance was correlated to an adjacent $H(PPh_3)$ resonance in a 2D NMR experiment (NOESY; *vide infra*, Spectroscopy section). Although intrinsically imprecise, the apparent $Fe_1$–$H_1$ and $Fe_4$–$H_1$ bond lengths [both 1.82(5) Å] are slightly elongated compared with the bridging Fe–H–Fe bond distances [1.668(4)

Table 1 Selected bond distances (Å) for the five-iron clusters **4**, **5**, **8**, $Fe_5C(CO_{15})$,[32] $Fe_5C(CO_{11})(PhMe_2P)_3$ ref. 20 and $(NMe_4)[Fe_5C(CO_{14})]$ [32]

| | Bond | 4 | 5 | 8 | $Fe_5C(CO_{15})$ | $Fe_5C(CO_{12})(PhMe_2P)_3$ | $[Fe_5C(CO_{14})]^{2-}$ |
|---|---|---|---|---|---|---|---|
| Fe-($\mu_5$-C) | $Fe_1$–$C_1$ | 1.888(8) | 1.859(3) | 1.897(10) | 1.875(8) | 1.858 | 1.882(13) |
| | $Fe_2$–$C_1$ | 1.874(8) | 1.852(3) | 1.867(10) | 1.897(7) | 1.876 | 1.866(14) |
| | $Fe_3$–$C_1$ | 1.932(8) | 1.879(3) | 1.932(10) | 1.865(8) | 1.868 | 1.853(13) |
| | $Fe_4$–$C_1$ | 1.899(8) | 1.857(3) | 1.876(10) | 1.893(7) | 1.868 | 1.862(14) |
| | $Fe_5$–$C_1$ | 1.949(7) | 2.015(3) | 1.978(10) | 1.948(7) | 2.022 | 1.993(13) |
| Fe–Fe | $Fe_1$–$Fe_2$ | 2.7998(15) | 2.7018(6) | 2.728(2) | 2.6331(15) | 2.656 | 2.657(3) |
| | $Fe_1$–$Fe_4$ | 2.7362(15) | 2.6450(6) | 2.681(2) | 2.6496(15) | 2.642 | 2.506(3) |
| | $Fe_1$–$Fe_5$ | 2.6285(15) | 2.5923(6) | 2.5937(19) | 2.557(16) | 2.579 | 2.637(3) |
| | $Fe_2$–$Fe_3$ | 2.6341(16) | 2.5757(6) | 2.628(2) | 2.6703(15) | 2.622 | 2.651(3) |
| | $Fe_2$–$Fe_5$ | 2.6045(16) | 2.6400(6) | 2.623(2) | 2.5869(15) | 2.651 | 2.579(3) |
| | $Fe_3$–$Fe_4$ | 2.6326(16) | 2.5552(6) | 2.624(2) | 2.6780(15) | 2.585 | 2.692(3) |
| | $Fe_3$–$Fe_5$ | 2.6248(16) | 2.5949(6) | 2.590(2) | 2.6466(16) | 2.643 | 2.594(3) |
| | $Fe_4$–$Fe_5$ | 2.6014(16) | 2.5937(6) | 2.619(2) | 2.5997(14) | 2.544 | 2.607(3) |
| Fe–P | $Fe_1$–$P_1$ | 2.2880(18) | 2.2245(8) | 2.261(3) | — | 2.263 | — |
| | $Fe_2$–$P_2$ | — | — | — | — | 2.324 | — |
| | $Fe_3$–$P_3$ | — | — | — | — | 2.248 | — |
| (μ5-C)-$plane_{Fe_4}$ | $C_1$–$Fe_4$ | 0.145 | 0.183 | 0.18 | 0.09 | 0.20(1) | 0.18 |
| Fe–H | $Fe_1$–$H_1$ | — | 1.82(5) | — | — | — | — |
| | $Fe_4$–$H_1$ | — | 1.83(5) | — | — | — | — |

and 1.670(4) Å] determined by neutron diffraction in the neutral four-iron cluster $[Fe_4(\eta_4\text{-CH})(CO)_{12}(\mu_2\text{-H})]$.[4]

The $PPh_3$-substituted iron site in **5** is—as in **4**—an equatorial iron, and the $PPh_3$ is similarly located below the basal plane.[7,20] The $Fe_1$–$P_1$ bond in **5** [2.2245(8) Å] is slightly shorter than that in neutral **4** [2.2880(18) Å]. The shorter bond in **5** is attributed to the anionic charge and the corresponding increase in iron oxidation states, namely an average of +0.8 in **4** *versus* +1.0 in **5**. Relatedly, the nitride cluster $[Fe_5(\mu_5\text{-N})(CO)_{13}(PPh_3)]^-$ reported by Berben *et al.*—also PSEPT 74 $e^-$ like **4** and **5**—exhibits an intermediate Fe–P bond length [2.2472(15) Å].[7] This is attributable to the combined effects of the nitride cluster's same $1^-$ charge (like cluster **5**), yet a lower iron oxidation state (+0.8 as with **4**). Overall, the adjacency of the hydride to the $PPh_3$–$Fe_1$ unit is rationalized according to the stabilization of the hydride by the most electropositive iron site.

Regarding the carbide, the $C_1$–$Fe_5$(apical) bond length in **5** [2.015(3) Å] is elongated as compared with **4** [1.949(7) Å]. This correlates with the greater carbide displacement ($d$) from the basal plane in **5** ($d = 0.183$ Å) compared with that in **4** ($d = 0.147$ Å). In an unexpected fashion, the combined effect (overall charge and phosphine ligation) in **5** on carbide displacement is less than that observed in the neutral, tri-substituted $Fe_5(\mu_5\text{-C})(CO)_{12}(PMe_2Ph)_3$, which exhibits a larger displacement ($d$ = 0.20 Å). Indeed, the binding of $PPh_3$ and hydride in mono-anionic **5** results in a similar carbide displacement as found in the di-anionic cluster $[Fe_5(\mu_5\text{-C})\mu_2\text{-}(CO)_2(CO)_{12}]^{2-}$ (0.18 Å).[20,32] Furthermore, the importance of ligand identity over cluster charge is underscored in the case of the cluster $Fe_5(\mu_5\text{-C})\mu_2\text{-}SO_2(CO)_{13}$, whose π acidic $SO_2$ ligand leads to a much smaller carbide displacement of $d = 0.10$.[15]

**$[Fe_3(\mu_3\text{-CH})(\mu_3\text{-CO})(CO)_9]_2[(bdpb)_2Fe(MeCN)_2]$ (6).** Compound **6** (Fig. 4) features the co-crystallized ion pair of two anionic, tri-iron methylidene carbonyl clusters with one cationic monometallic, octahedral bis(diphosphine)Fe(II) complex. The methylidene cluster, as with the tri-iron unit of **6**, is structurally similar to the literature structure.[40] The Fe(II) species $[Fe(MeCN)_2(bdpb)_2]^{2+}$ unit exhibits four phosphines in the equatorial plane and two axial MeCN ligands coordinated *trans* to each other, and it is analogous to the ferrous complex $[Fe(MeCN)_2(bdpb)_2]^{2+}$ reported by Barclay.[41] Similar to the 'clipping' ability of Triphos in **10**, this structure demonstrates that constrained bis-chelating ligands are sterically disposed to binding a single iron site, which causes dissociation of a single-site Fe's from the cluster framework; the remainder is a lower

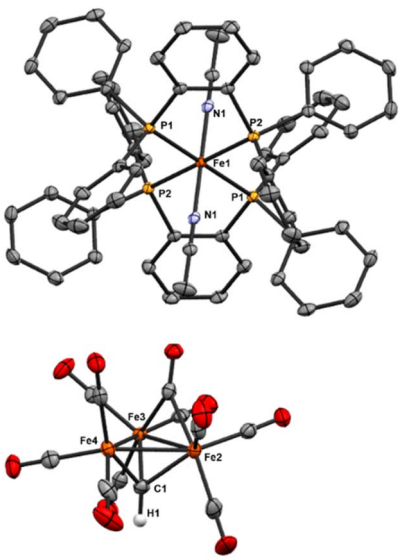


Fig. 4 ORTEP diagram (50% thermal ellipsoids) of $[Fe_3(\mu_3\text{-CH})(\mu_3\text{-CO})(CO)_9]_2[(bdpb)_2Fe(MeCN)_2]$ (**6**); H atoms are omitted for clarity except for the $\mu_3$-CH. It is shown as a grown structure of the asymmetric unit cell, equivalent P and N atoms are labeled, and only one of the two equivalent anions is shown.

nuclearity iron-carbide cluster (*i.e.* the anion in **6**) that is essentially intact.

**$Fe_5(\mu_5\text{-}C)(CO)_{14}(\kappa_1\text{-Triphos})$ (8).** The substitution of a single Triphos arm onto the *nido* iron cluster in **8** (Fig. 5) was unexpected. While the structural motif of a doubly bonded Triphos at a single metal center (with a single unbound phosphine arm) is relatively common (31 examples in CCDC), a search including a $\kappa_1$-Triphos motif afforded no results. As in **4**, the basal plane coordination mode matches the literature precedent. However, the carbide displacement in **8** (0.18 Å) is larger than that found in **4** [0.145 Å]—which is also a neutral, singly phosphine-substituted cluster. The carbide displacement is much greater than that predicted by literature trends, instead being comparable to the dianionic $[Fe_5(\mu_5\text{-}C)\mu_2\text{-}(CO)_2(CO)_{12}]^{2-}$, the tri-substituted neutral cluster $Fe_5(\mu_5\text{-}C)(CO)_{12}(PMe_2Ph)_3$, and the monoanionic monosubstituted **5** [0.18, 0.20(1) and 0.183 Å, respectively] rather than the more structurally and electronically analogous neutral **4**. Provided that the diphenyl-substituted Triphos is not significantly more σ-donating than $PPh_3$, we attribute this distortion to the steric constraints of the bulky Triphos binding rather than the electronics of the bound ligand.

**$[Fe_4(\mu_4\text{-}C)(\mu_2\text{-}CO)_2(CO)_8(\kappa_3\text{-Triphos})]$ (9).** The coordination of the three Triphos phosphine arms in **9** (Fig. 6) exhibits distinct regioselectivity from that reported for multiple monophosphine coordination onto $Fe_4(\mu_4\text{-}C)(CO_{13})$, as well as the related nitride cluster $[Fe_4(\mu_4\text{-}N)(CO_{12})]^-$. In **9**, one iron site is chelated in a bidentate fashion by two Triphos arms, rather than each phosphine donor coordinating a separate iron site. There are no such $Fe_4$-carbide 'butterfly' clusters with multiple ligated phosphines in the CCDC. However, Bradley reported partial structural data for the triply substituted species $Fe_4(\mu_4\text{-}C)(\mu_2\text{-}CO)(CO)_9(PMe_3)_3$ and partial spectroscopic data for a proposed quadruply substituted cluster $Fe_4(\mu_4\text{-}C)(CO)_8(PMe_3)_4$. In each case, the $PMe_3$ ligands bind at discrete iron sites—unlike the single metal site chelation on $Fe_2$ observed in **9**. The triply substituted $Fe_4(\mu_4\text{-}C)(\mu_3\text{-}CO)(CO)_9(PMe_3)_3$ species contrasts with our chelated, triply substituted cluster **9**.[21]

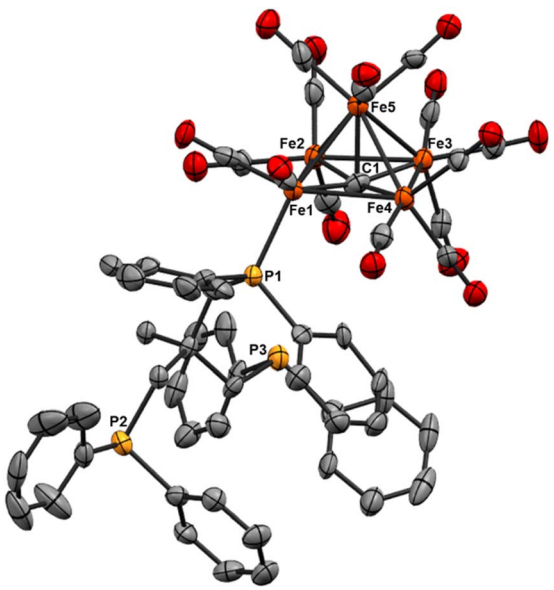


Fig. 5 ORTEP diagram (50% thermal ellipsoids) for the mono-substituted $Fe_5$ cluster $Fe_5(\mu_5\text{-}C)(CO)_{14}$(Triphos) (**8**); H atoms are omitted for the sake of clarity.

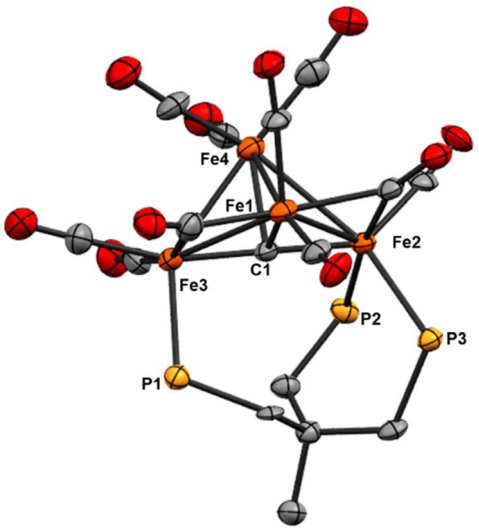


Fig. 6 ORTEP diagram (50% thermal ellipsoids) for the tri-substituted $Fe_4$ cluster $Fe_4(\mu_4\text{-}C)(\mu_2\text{-}CO)_2(CO)_8(\kappa_3$-Triphos) (**9**); H atoms and phenyl rings are omitted for the sake of clarity.

The location of the phosphine donors on the 'wing-tip' iron sites ($Fe_2$ and $Fe_3$) is consistent with most literature studies (Fe-nitride clusters). However, the wing-tip motif is slightly different from the triply $PMe_3$ ligated Fe-carbide cluster reported by Bradley,[21] which exhibits only one wing-tip $PMe_3$ and two $PMe_3$ in the basal locations. The orientation of the phosphine donors above the axial $Fe_2$–$C_1$–$Fe_3$ motif is also consistent with the reported $Fe_4$ structures (Table 2).[21,22,42,43]

Finally, we speculate that the coordination of three phosphine ligands onto the two wing-tip irons in **9** thermodynamically destabilizes the cluster core, an effect primarily compensated for by multi-iron chelation. The 'cluster chelation' prevents (immediate) cluster disproportionation, but may not completely compensate for the unsymmetrical Fe electronics as evidenced by the eventual formation of the phenyl-transfer product $[Fe_3(\mu_3\text{-}CPh)\{Triphos(PPh_2)_2(PPh)\}(CO)_7]$ (**11**) and mononuclear (Triphos)$Fe(CO)_2$.

**$[(CO)_9Fe_3(\mu_3\text{-}CCO_2\text{-}\kappa_2)Fe(CO)(\kappa_3\text{-Triphos})]$ (10).** The 'clipped iron' structure **10** (Fig. 7) exhibits a tri-iron cluster linked to a monometallic, pseudo-octahedral Fe(II) center that is bridged through the $\kappa_3$-$CCO_2$ unit and capped by Triphos. The $\mu_3$-carbon unit has been reported as a linking motif as in the 'dimeric' cluster $[Fe_3(CO)_9\{\mu_3\text{-}C(\mu_2\text{-}C)_2C\text{-}\mu_3\}Fe_3(CO)_9]^{2-}$, as well as the analogous linking of clusters with mononuclear metal sites.[44–48]

The $Fe_3(CO)_8(\mu_3\text{-}CO)(\mu_3$-aceto-$\kappa_2$-O) cluster unit in **10** (Fig. 7) is unique in the CCDC, although several similar structures have been reported with generalized $\mu_3$-CR moieties, such as $Fe_3(CO)_8(\mu_3\text{-}CCH_3)(\mu_3\text{-}COCH_3)$ reported by Hursthouse in 1983.[49] The cluster $NEt_4[Fe_3(CO)_8(\mu_3\text{-}CO)(\mu_3\text{-}CCH_3)]$ was

Table 2 Selected bond distances (Å) and angles (°) for the four-iron clusters **9**, $Fe_4C(CO_{13})$,[18] $Fe_4C(CO)_{10}(PMe_3)_3$,[21] $[Fe_4(CH)(CO_{12})(PPh_3)H]^-$,[22] and $[Fe_4C(CO_{12})]^{2-}$ [23]

| | Bond or angle | **8** | $Fe_4C(CO)_{13}$ | $Fe_4C(Co)_{10}(PMe_3)_3$ | $[Fe_4(CH)(CO)_{12}(PPh_3)H]^{1-}$ | $[Fe_4C(CO)_{12}]^{2-}$ |
|---|---|---|---|---|---|---|
| Fe-($\mu_4$-C) | $Fe_3$–$C_1$ | 1.813(7) | 1.797(4) | 1.838(4) | 1.908(7) | 1.810(7) |
| | $Fe_1$–$C_1$ | 1.962(7) | 1.999(4) | 1.979(4) | 1.926(9) | 1.969(5) |
| | $Fe_4$–$C_1$ | 1.943(7) | 1.988(4) | 2.104(4) | 1.973(8) | 1.969(5) |
| | $Fe_2$–$C_1$ | 1.801(7) | 1.800(4) | 1.758(4) | 1.973(8) | 1.786(7) |
| Fe–Fe | $Fe_3$–$Fe_1$ | 2.6332(15) | 2.624(1) | 2.644(19) | 2.669(2) | 2.637(1) |
| | $Fe_3$–$Fe_4$ | 2.6326(16) | 2.637(1) | 2.644(19) | 2.613(2) | 2.637(1) |
| | $Fe_1$–$Fe_2$ | 2.6016(15) | 2.647(1) | 2.644(19) | 2.630(2) | 2.653(1) |
| | $Fe_4$–$Fe_2$ | 2.7028(16) | 2.640(1) | 2.644(19) | 2.624(2) | 2.653(1) |
| | $Fe_1$–$Fe_4$ | 2.5287(15) | 2.545(1) | 2.528(1) | 2.584(2) | 2.534(1) |
| Fe–P | $Fe_3$–$P_1$ | 2.247(2) | — | Not reported | 2.238(2) | — |
| | $Fe_2$–$P_2$ | 2.269(2) | — | Not reported | — | — |
| | $Fe_2$–$P_3$ | 2.2545(19) | — | Not reported | — | — |
| Wing torsion | Dihedral | 102.17 | 101 | 102.4 | 107.55 | 101 |
| $Fe_2$–$C_{carbide}$–$Fe_3$ | $Fe_2$–$C_1$–$Fe_3$ | 175.3(4) | 175 | 174 | 172.4(5) | 178 |

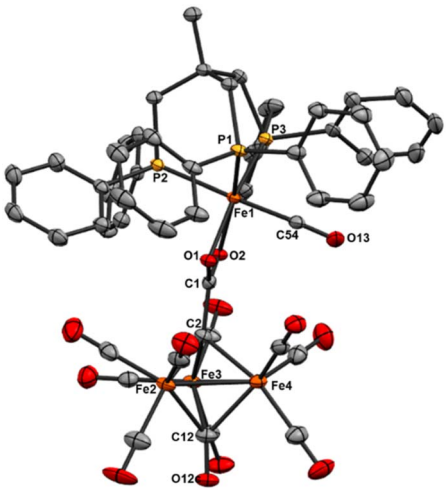


Fig. 7 ORTEP diagram (50% thermal ellipsoids) for the 'clipped' cluster $[Fe_3(CO)_8(\mu_3\text{-}CO)(\mu_3\text{-aceto-}\kappa_2O)Fe(CO)(\kappa_3\text{-Triphos})]$ (**10**). The detached Fe(II)–CO site is 50% occupied by MeCN in the crystal lattice; a disordered solvent molecule (toluene) and H atoms are omitted for the sake of clarity.

reported by Zacchini more recently, and also features the same $\mu_3$-CO found in **10**.[40] The Fe–Fe bond distances in **10** are similar to those found in the Hursthouse cluster (Fe–$Fe_{avg}$ 2.2559 Å *vs.* 2.520 Å, respectively). Ultimately, the similarity of the cluster core bond metrics of **10** with reported clusters suggests that the tri-iron subunit of the 'clipped' structure **10** is mostly unaffected (electronically) by the linked monometallic site.

The coordination geometry of the detached ferrous site is best compared with the Fe(II) complexes of tri-sphosphinephenylborate (aka $\mathbf{BP_3^R}$) complexes reported by Peters, namely monomeric $[(\mathbf{BP_3^R})Fe(\text{acetato-}\kappa_2O)]$ and dimeric $\mu_2$-oxalato-$(\kappa_2O)_2$-$[(\mathbf{BP_3Cy})Fe(CO)]_2$.[50,51] In contrast to these structures, the sixth coordination site in **10** is occupied by CO and MeCN (1 : 1, crystallographically). The Fe–P, Fe–C(aceto) and Fe–CO bond lengths are all similar. Ultimately, this structural result demonstrates that Triphos can (thematically) 'clip' a single iron site from the progenitor $Fe_4$ cluster framework.

**$[Fe_3(\mu_3\text{-CPh})\{\text{Triphos}(PPh_2)_2(PPh)\}(\mu_2\text{-CO})_2(CO)_5]$ (11).** Cluster **11** (Fig. 8) gives insight into the intramolecular phenyl transfer from a Triphos-$PPh_2$ unit (intact in **9**) to the interstitial carbide (thus forming a $\mu_3$-C(Ph) unit), with stoichiometric loss of a basal $Fe(CO)_3$ unit. The resulting product is a three-iron cluster with an anionic phosphide ($RPhP^-$), which bridges the two iron sites directly supported by the two remaining (intact) $Ph_2P$ donors of Triphos. The phosphide bond distances [$P_3 - Fe_1 = 2.2010(5)$ and $P_3 - Fe_2 = 2.2116(5)$ Å] are slightly shorter than the two Triphos–$PPh_2$ bond distances [$P_1 - Fe_1 = 2.2663(5)$ and $P_2 - Fe_2 = 2.2334(5)$ Å]. Overall, cluster **11** demonstrates that the interstitial carbide is not rendered chemically inert by Triphos ligation.

## Spectroscopic characterization (NMR and IR)

### Six-iron cluster

*$Fe_6(\mu_6\text{-}C)(\mu_2\text{-}CO)(CO)_{17}$.* The $\nu$(CO) features in the IR of **3** are essentially equivalent to those of the *nido*-five iron compound

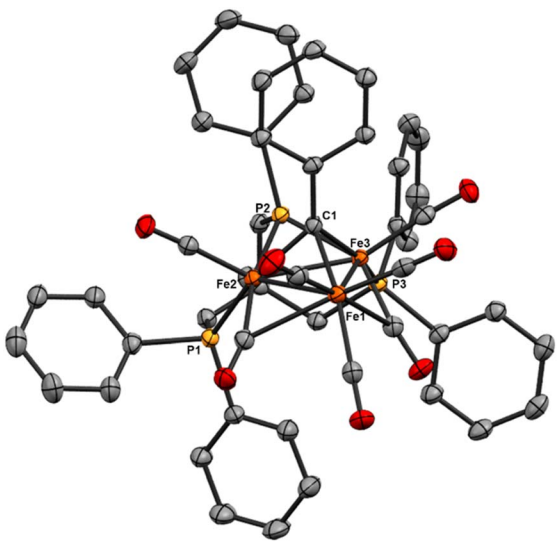


Fig. 8 ORTEP diagram (50% thermal ellipsoids) for the 'clipped' cluster $[Fe_3(\mu_3\text{-CPh})\{\text{Triphos}(PPh_2)_2(PPh)\}(\mu_2\text{-CO})_2(CO)_5]$ (**11**). A disordered solvent molecule (toluene) and H atoms are omitted for the sake of clarity.

$Fe_5(\mu_5\text{-C})(CO)_{15}$ with a leading feature at 2095, and dominant peaks at 2018, 1994, 1973, and 1941. The notable difference is a medium-intensity feature at 1821 $cm^{-1}$ correlated with the single bridging carbonyl in the crystal structure. $^{13}$C-NMR shows multiple resonances in the carbonyl region at 212.24, 21.11, and 209.45 ppm.

**Five-iron clusters**

*$Fe_5(\mu_5\text{-C})(CO)_{14}(PPh_3)$ (**4**).* The IR spectrum of **4** exhibits a red-shift in its leading $\nu$(CO) feature (2078 $cm^{-1}$) compared with the analogous feature at 2097 $cm^{-1}$ in the unsubstituted analog $Fe_5(\mu_5\text{-C})(CO)_{15}$. This is consistent with the substitution of a strong $\pi$-acceptor (CO) for a $\sigma$ donating but relatively electron-poor phosphine and is in accordance with the report from Cooke and Mays.[19] Additionally, the increased number of $\nu$(CO) features in **4** relative to the unsubstituted cluster indicates a decrease in the symmetry of the *nido* cluster **4** upon phosphine substitution for CO (see Table S1†). This is further supported by the increased relative intensity of the leading feature at 2078 $cm^{-1}$. We posit that the medium intensity, sharp leading feature at 2078 $cm^{-1}$ is Raman active and IR forbidden in symmetric, unsubstituted clusters such as $Fe_5(\mu_5\text{-C})(CO)_{15}$, which shows only a very weak but sharp feature, possibly thermally allowed, at 2098 $cm^{-1}$. This stretch is symmetry allowed by the newly imposed asymmetry of phosphine binding, and we observed a similar effect in the case of **5** and **8** with their analogous features at 2041 and 2078 $cm^{-1}$, respectively. The $^{31}$P NMR spectrum exhibits a resonance at 53.73 ppm that is consistent with a metal-bound phosphine, as well as a resonance corresponding to unbound phosphine. We posit that this indicates only dynamic ligation in the solution state. The participation of phosphine ligands in intramolecular ligand exchange on iron carbonyl clusters has been reported by Wadepohl previously.[22] Interestingly, the $^{13}$C NMR spectrum of $Fe_5(\mu_5\text{-C})(CO)_{14}(PPh_3)$ in $C_6D_6$ exhibits a carbide resonance at 490.11 ppm, slightly deshielded relative to the reported 486.0 ppm resonance for the neutral, unsubstituted cluster $Fe_5(\mu_5\text{-C})(CO)_{15}$.[32]

*$NEt_4[Fe_5(\mu_5\text{-C})(\mu_2\text{-H})(CO)_{13}PPh_3]$ (**5**).* The IR spectrum of **5** exhibits both terminal $\nu$(CO) peaks and multiple bridging $\nu$(CO) peaks, consistent with the CO binding modes and overall symmetry observed in the crystal structure (Table S1†). The $^{31}$P NMR spectrum exhibits a single resonance at 62.17 ppm, consistent with a metal-bound phosphine, thus indicating that the structure in solution is consistent with the crystal structure. The resonance shift is deshielded relative to the neutral analog **4**, which is consistent with the expectation for an anionic cluster. The proposed assignment of a bound hydride in the X-ray structure is fully supported by the $^1$H NMR spectrum, which exhibits a hydride resonance at −11.71 and −11.75 ppm (doublet, $J$ = 24 Hz). For comparison, the six-iron, tri-anionic hydride cluster $[Fe_6(\mu_6\text{-C})(\mu_2\text{-H})(CO)_{15}]^{3-}$ reported by Zacchini *et al.* features a hydride resonance at −20.7 ppm; this suggests that the more downfield resonance for our monoanionic, lower nuclearity cluster is reasonable given the comparatively weaker shielding effect expected in the less strongly charged five-iron cluster.[52] NOESY analysis reveals coupling between the −11.71 and −11.75 ppm resonance and aryl peaks from $PPh_3$, supporting the structural assignment of the hydride location bridging between $Fe_1$ and $Fe_4$, adjacent to the $PPh_3$ binding site on $Fe_1$. The $^{13}$C NMR of $NEt_4[Fe_5(\mu_5\text{-C})(\mu_2\text{-H})(CO)_{13}PPh_3]$ in $d_3$-MeCN exhibits a carbide resonance at 488.63 ppm. This is unexpected, as it is more similar to the neutral, $PPh_3$ substituted cluster (490.11 ppm) than to other charged clusters. We speculate that ligand and hydride substitution induces chemical and symmetry changes to the cluster that have a greater influence on the carbide $^{13}$C resonance than the overall cluster electronics, which contradicts the previously reported literature explanation.

*$Fe_5(\mu_5\text{-C})(CO)_{14}$(Triphos) (**8**).* As in the other mono-substituted five-iron cluster **4**, the $^{31}$P NMR spectrum of **8** exhibits a labile Triphos ligand, even in a non-coordinating solvent such as deuterated benzene.

The spectrum features six dominant resonances, one of which integrates ∼50:1–3 with the other five. We expected two or three, one indicating bound phosphine, and the others the free Triphos arms. We speculate that these additional, persistent (by repeated column purification) resonances are attributable to variable binding modes of the three Triphos arms occurring transiently in solution (see Fig. S25.†) The spectrum is dominated by a resonance at −25.64 ppm, which corresponds to free Triphos, likely a combination of some excess Triphos contamination and complete ligand dissociation in solution.

The carbide resonance at 489.33 ppm is deshielded in a similar fashion relative to $Fe_5(\mu_5\text{-C})(CO)_{15}$—to a similar extent to cluster **4**. Also similar to cluster **4**, cluster **8** possesses only terminal carbonyls, with the leading IR feature at 2078 $cm^{-1}$, a similar red-shift relative to the spectrum of $Fe_5(\mu_5\text{-C})(CO)_{15}$ as that of **4** at 2079 $cm^{-1}$. This indicates that despite the lability–and likely the variable binding motifs–of the phosphine in solution, it has a notable impact on the electronics and is analogous to $PPh_3$ binding. The asymmetry induced by mono-phosphine binding of the sterically encumbered Triphos ligand on a single equatorial iron vertex is also observable in the $\nu$(CO) features. In this case, a moderately intense and sharp feature appears at 2078 $cm^{-1}$, with broad, prominent features at 2011 and 1995 $cm^{-1}$. As with **4**, we attribute the presence of this peak to the breaking of pure $O_h$ symmetry in the cluster.

**Four-iron cluster**

*$Fe_4(\mu_4\text{-C})(\mu_2\text{-CO})_2(CO)_8(\kappa_3\text{-Triphos})$ (**9**).* The $^{13}$C NMR carbide resonance of **9** is distinct from that of the neutral tetra-iron carbide cluster, $Fe_4(\mu_4\text{-C})(CO)_{13}$, at 485.34 ppm (*versus* 468.9 ppm in the unsubstituted cluster).[21,52] The downfield shift indicates a significantly different carbide environment after Triphos ligation. Interestingly, the shift downfield with Triphos ligations as compared to the neutral, unsubstituted cluster is more extreme ($\Delta\delta$ = 16.44 ppm) than that reported for the tetra-substituted $Fe_4C(CO)_9(PMe_3)_4$ ($\Delta\delta$ = 2.6 ppm), despite the lower extent of CO substitution and the comparative electron deficiency of Triphos donors relative to $PMe_3$. This is a greater downshift than that induced by 2 $e^-$ cluster reduction ($\Delta\delta$ = 9.1 ppm) (Table 3). It is unclear if non-bonding interactions between the exposed carbide and the 3 Å distal Triphos scaffold

Table 3 $^{13}$C NMR resonances and displacement from the basal 4Fe plane of the interstitial carbide in five-iron carbide clusters from this work

| | $Fe_5C(CO_{15})$[a] | $[Fe_5C(CO_{14})]^{2-}$[b] | $Fe_5C(CO_{12})(PMe_2Ph)_3$ | **4** | **5** | **8** |
|---|---|---|---|---|---|---|
| $\mu_5$-C ($\delta$ in ppm) | 486.0 | 475 | Not reported | 490.11 | 488.63 | 489.33 |
| $\Delta$C–$Fe_4$ plane (Å) | 0.09 | 0.18 | 0.20 | 0.145 | 0.183 | 018 |

[a] Kaupp *et al.*[52] [b] Kuppuswamy *et al.*[32]

Table 4 Interstitial carbide $^{13}$C NMR shifts for tetra-iron clusters

| | Dihedral $\delta$ (°) | Fe–C–Fe (°) | $\mu_4$-C $^{13}$C NMR (ppm) |
|---|---|---|---|
| $Fe_4C$ Triphos | 102.17 | 175.31 | 485.34 |
| $Fe_4C(CO)_{13}$ | 101[a] | 175[a] | 468.9[b] |
| $Fe_4c(CO)_{10}(PMe_3)_3$ | 102.4[a] | 174[a] | Not reported |
| $Fe_4C(CO)_9(PMe_3)_4$ | Not reported | Not reported | 471.5[a] |
| $[Fe_4(C)(CO_{12})H]^-$ | 104[a] | 174[a] | 464.2[a] |
| $[Fe_4C(CO_{12})]^{2-}$ | 101[a] | 178[a] | 478.0[a] |

[a] From Bradley *et al.*[21] [b] Kaupp *et al.*[52]

induce further deshielding. Indeed, the reduction and protonation of the $Fe_4$ cluster to generate monoanionic $[Fe_4C(CO_{12})H]^-$ result in the opposite effect, with an upfield shift of 4.7 ppm (Table 4).

Unlike $Fe_5(\mu_5\text{-C})(\kappa_1\text{-Triphos})(CO)_{14}$ (**8**), the $^{31}$P NMR spectrum exhibits two dominant resonances: a broad singlet at 49.70 ppm and a sharp singlet at −24.67 ppm; these two resonances integrate 1 : 2. We posit that this reflects two phosphine arms being consistently unbound in solution, generating an undercoordinated and thus reactive cluster species. This is consistent with the observed formation of **11** from **9** over time in solution *via* a reaction between the carbide and a phosphine arm. It is conceivable that the observed reactivity (*vide supra*), whereby the carbide is reactive in the parent cluster $Fe_4(\mu_4\text{-C})(CO)_{13}$ but not in **9**, is explained by Triphos coordination over the butterfly carbide face sterically protecting the otherwise reactive carbide in non-coordinating solvent.

The IR spectrum of **9** exhibits eight sharp features in the $\nu$(CO) 'neutral carbonyl cluster' region (2050–1900 cm$^{-1}$ for terminal CO and ∼1800 cm$^{-1}$ for bridging), at 2059, 2042, 2035, 1971, 1944, 1918, (terminal) and 1884 and 1799 cm$^{-1}$ (bridging). Such features closely parallel the CO binding motifs observed in the crystal structure. Multiple sharper features—rather than the commonly broad $\nu$(CO) peaks in more symmetric clusters—are likely a result of the decreased symmetry upon Triphos binding.

### Computational investigation of the non-PSEPT intermediate (2)

**Computational structure.** The proposed, meta-stable, neutral cluster $[Fe_6(\mu_6\text{-C})(CO)_{16}]$ (**2**) readily disproportionates and either has a reactive interstitial carbide that generates the $Fe_3C(R)$ clusters (**7**, **10**, **11**, *etc.*), or it generates reactive cluster fragments in solution. The previously reported (also neutral) six-iron cluster, $Fe_6(\mu_6\text{-C})(CO)_{18}$ (isolated, but not structurally characterized), was geometry-optimized (B3PW91/6-31G) as a *nido*-pentagonal structure, exhibiting a drastic distortion of the four-iron equatorial plane. We thus anticipated that the *in situ*-oxidized, meta-stable neutral $[Fe_6(\mu_6\text{-C})(CO)_{16}]$ would present a similar equatorial distortion that would raise the energy of the carbide frontier orbitals closer to that of the frontier molecular orbitals of the cluster. We also observed that the oxidation of $[Fe_6(\mu_6\text{-C})(CO)_{16}]^{2-}$ generates the neutral species **2** in both coordinating and noncoordinating solvents, strongly indicating that the cluster does not bind solvent prior to the addition of the intended external ligands ($PPh_3$, Triphos, *etc.*). Cluster **2** is stable on the minutes-to-hours timescale (depending on solvent and temperature), and the IR spectrum in all cases exhibits a $\nu$(CO) feature that is consistent with a neutral cluster species (1990 cm$^{-1}$, broad and intense). We were thus motivated to simulate a putative structure of **2** using validated DFT methods (*vide infra*, five-iron cluster) to determine the structural characteristics of this metastable, non-PSEPT ($14n$, where $n = 6$, thus 84 e$^-$) cluster.

**Validation of density functional theory methods for the modeling of five- and six-iron carbide carbonyl clusters.** Computational analysis of transition metal carbonyl clusters presents particular challenges. One is simply the computational cost introduced by the multitude of metal centers. Other challenges include the significant extent of M($d$)|CO($\pi$*) back-bonding and the structural variety of $M_n$–CO bonds (terminal, bridging, and semi-bridging), the metal–metal interactions as the cluster size increases, and the varying cluster charges; indeed to the latter point, the known six-iron carbide carbonyl clusters range from neutral to 4$^-$.[32,52]

Density functional methods used in the literature on iron carbonyl carbide clusters have varied, depending on the application. Debeer & Holland and coworkers modeled the charged and neutral versions of six-iron-carbide, nitride, and oxide carbonyl clusters. They used the BP86 functional and a combination of basis set families, a dense integration grid, and the dielectric continuum model (COSMO) to model electronic structures and XES and XAS spectra. Zacchini and coworkers modeled the electronic structures and relative Gibbs free energy values of di- and tetra-anionic iron carbide carbonyl clusters and their proposed intermediates using the range-separated functional ωB97-x, Ahlrich's basis set family, and a C-PCM implicit solvent model.[52] Our group previously performed geometry optimization on neutral six-iron clusters using the hybrid B3PW91 functional and Pople basis sets.[32] In another report from DeBeer and coworkers in collaboration with our group, anionic iron and iron-molybdenum carbonyl clusters were modeled using B3LYP, Ahlrichs and CP(PPP) basis sets for the calculation of their Mössbauer parameters.[53] An important distinction between previous examples and the challenge reported herein of structurally predicting **2** is that most literature

 

precedent is premised upon a structurally characterized cluster. Due to a lack of crystal structures, our computational approach thus required rigorous validation. However, to our knowledge, no rigorous validation or benchmarking studies on iron-carbide-carbonyl clusters have been reported. Therefore, we endeavored to select and validate a computational toolkit suitable to approach this family of clusters. These methods are detailed in the ESI,† and the key conclusions are discussed below.

Accuracy in the modeling of transition metal compounds is dependent on the extent of Hartree–Fock (HF) contribution and the type of metal-ligand system.[54] We selected functionals from available literature: B3LYP,[53] BP86,[55] ωB97-x[52] and B3PW91;[32] these functionals utilize an increasing percent of HF contribution (0–20%, Table S14†). For this purpose, we also tested 15% HF contribution versions of two hybrid functionals, B3LYP-15. Separately, we selected the minimally augmented versions from the Ahlrichs basis set family in light of their widespread use for transition metals, as well as iron-carbide carbonyl specifically (see details in the ESI†).[52,53,55]

We selected the optimal functional and basis set for geometry optimization of **2** by determining the accuracy of several functionals using the closely related (also neutral) and structurally characterized neutral cluster $Fe_5(\mu_5\text{-}C)(CO)_{15}$ (Tables S11 and S12†). Multiple combinations of functional and basis sets provided reasonable results in terms of structural RMSD and selected bond lengths between $[Fe_5(\mu_5\text{-}C)(CO)_{15}]_{X\text{-}ray}$ and $[Fe_5(\mu_5\text{-}C)(CO)_{15}]_{DFT}$ (Tables S16 and S17†) and vibrational analysis (Tables S18–S21 and Fig. S50–60†). Among them, the BP86-D4/TZVP combination provided a converged gas-phase geometry of **2** with only small (less than 100 $cm^{-1}$) imaginary frequencies (Fig. 9).

The evaluated imaginary frequencies emanated from 'breathing modes' involving all cluster atoms. To eliminate these frequencies, small, randomized distortions of the starting coordinates followed by re-optimization were attempted, including increasing the optimization threshold and increasing the angular integration grid number. None of the established methods for resolving imaginary frequencies proved successful, so the parameters were re-evaluated. The literature precedent shows that charged clusters in this family can be modeled using the implicit solvation model C-PCM.[52,56,57] We thus returned to the validation compound $Fe_5(\mu_5\text{-}C)(CO)_{15}$ and evaluated the effect of C-PCM with a dielectric constant of 9.08 corresponding to dichloroethane. The optimized geometry with C-PCM was nearly identical to the same calculation performed without C-PCM; however, four carbonyls shifted from terminal motifs to structurally inaccurate bridging motifs (Fig. S61.†) The simulated vibrational spectrum reflects this and thus contradicts the experimental data (Table S23†). We further applied C-PCM with a range of dielectric constants aiming to eliminate the imaginary frequencies, but these calculations all provided essentially equivalent geometries and vibrational spectra (Tables S24 and S25†). Ultimately, the discrepancy between the experimental and simulated CO vibrational modes when C-PCM was applied to $[Fe_5(\mu_5\text{-}C)(CO)_{15}]_{DFT}$ indicated that optimization in the gas-phase would be most suitable for modeling **2** (*vide infra*). More generally, we concluded that the addition of C-PCM is inconsistent when used for modeling neutral iron-carbide carbonyl clusters. In contrast, preliminary computations using the anionic cluster **1** suggest that C-PCM is not only suitable but also necessary for convergence. [Note: such results on the anionic cluster(s) are outside the scope of this report.] Ultimately, the close agreement in bond metrics and vibrational spectra between $[Fe_5(\mu_5\text{-}C)(CO)_{15}]_{X\text{-}ray}$ and the gas-phase model $[Fe_5(\mu_5\text{-}C)(CO)_{15}]_{DFT}$ (Tables S16 and S17†) inspired confidence in the simulated geometry of $\mathbf{2}_{DFT}$ presented herein.

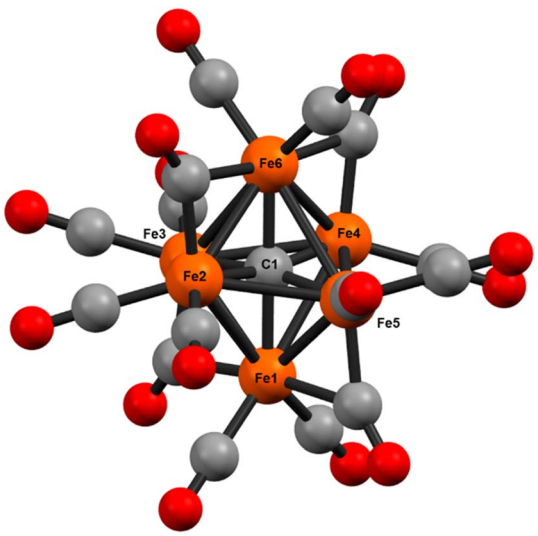


Fig. 9 Ball and stick model of the DFT (BP86/def2-TZVP) optimized geometry of the key synthetic intermediate $[Fe_6(\mu_6\text{-}C)(CO)_{16}]$ ($\mathbf{2}_{DFT}$) that enabled the synthesis of phosphine-supported iron-carbide clusters.

**Optimized geometry of (2).** The resulting geometry optimized structure of $\mathbf{2}_{DFT}$ (BP86/Ahlrichs, *vide supra*) (Fig. 9) is quite distinct from both the *closo* ($14n + 2$) structure of $[Fe_6(\mu_6\text{-}C)(CO)_{16}]^{2-}$ (**1**) and the *nido*-pentagonal ($14n + 4$) structure of $Fe_6(\mu_6\text{-}C)(CO)_{18}$.[32] The DFT prediction of the latter structure exhibits an '$Fe_7$-like' pentagonal bipyramidal framework, except that one Fe site is missing—thus producing a *nido*-pentagonal-bipyramidal structure. Structural analysis of dianonic **1** reveals a slightly distorted—but otherwise quite regular—$Fe_6$ framework that is tetragonally elongated in both DFT and X-ray structures. In contrast, the simulated $Fe_6$ framework of $\mathbf{2}_{DFT}$ retains the *closo* motif of $[Fe_6(\mu_6\text{-}C)(CO)_{16}]^{2-}$ (the same number of CO ligands and Fe–Fe bonds); this is expected for an electron deficient cluster [*arachno*: 90 $e^-$ ($14n + 6$) → *nido*: 88 $e^-$ ($14n + 4$) → *closo*: 86 $e^-$ ($14n + 2$) → *hypercloso*: 84 $e^-$ ($14n$, *vide infra* next paragraph)].[58,59] For example, the addition of two electrons upon going from *closo* (86 $e^-$) to *nido* (88 $e^-$) breaks one Fe–Fe bond. However, a 'ruffling' of the equatorial plane in $\mathbf{2}_{DFT}$ is quite apparent, thus deviating from the more regular (albeit tetragonally distorted) octahedral motif of $[Fe_6(\mu_6\text{-}C)(CO)_{16}]^{2-}$.

The formulation of the PSEPT electron counting for **2** is consistent with a *hypercloso* model in an analogous extension of PSEPT for metal clusters [*closo*: 86 $e^-$ ($14n + 2$) → *hypercloso*: 84 $e^-$ ($14n$)]. Similarly, some theoretical models of borohydride

clusters[60]—and limited examples of crystallographically characterized 6-borane and alane clusters[61,62]—can be formulated as '*hypercloso*'.[59,63,64] The geometric variation in the $Fe_6(\mu_6\text{-}C)$ core of $\mathbf{2_{DFT}}$ (compared with known 6-vertex *closo* and *nido* iron carbide clusters, including **3**) was analyzed *via* continuous shape analysis using the program SHAPES, which determines the ideality of a structure with respect to ideal polyhedra.[65] The $Fe_6(\mu_6\text{-}C)$ core of $\mathbf{2_{DFT}}$ was analyzed alongside the crystallographic coordinates of *closo* $[Fe_6(\mu_6\text{-}C)(CO)_{16}]^{2-}$ and *closo* $[Fe_6(\mu_6\text{-}C)(CO)_{15}]^{4-}$,[33] as well as **3** and the (previously)[32] DFT-calculated model for *nido* $Fe_6(\mu_6\text{-}C)(CO)_{18}$ (Fig. 10, Table 6). As expected, both anionic *closo* structures correlated strongly with an octahedron and produced the lowest deviation of the four structures (0.23 for each). Interestingly, the neutral *closo* cluster cores produced lower deviations, at 0.087 and 0.099. The *nido* cluster also resulted in a low deviation from octahedral (3.37), but with diminished fidelity compared to the *closo* examples; the *nido* cluster also exhibited a lower deviation from trigonal prism and pentagonal clusters (19.66 and 9.71, respectively). In contrast, $\mathbf{2_{DFT}}$ exhibits a lower deviation from octahedral clusters (0.60), as well as a lower deviation from trigonal prism and pentagonal pyramid clusters (14.11 and 26.77, respectively) compared with either the *closo* or the *nido* structures.

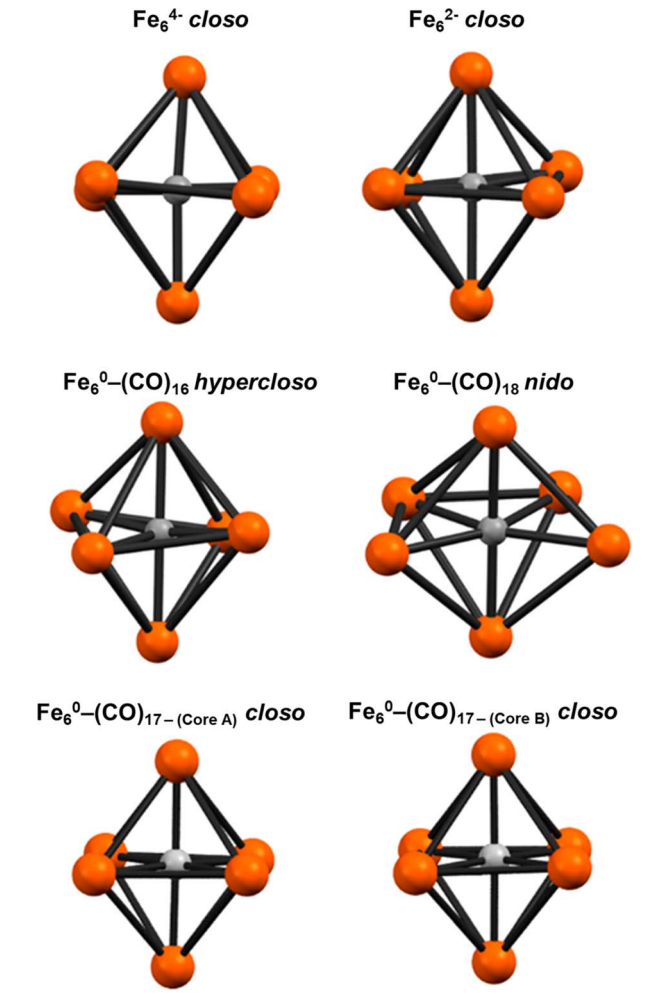


Fig. 10 Ball and stick models of the iron-carbide cores of the known six-iron clusters.

The axial Fe–C(carbide) bonds ($Fe_1$–$C_1$ and $Fe_6$–$C_1$ = 1.880 Å) in $\mathbf{2_{DFT}}$ are slightly shorter than the equatorial Fe–$C_1$ bonds (1.894 Å). This trend is similar to the iron-carbide bonds experimentally determined for $[Fe_6(\mu_6\text{-}C)(CO)_{16}]^{2-}$ (Table 5). The axial $Fe_1$–$C_1$–$Fe_6$ angle in $\mathbf{2_{DFT}}$ is exactly linear at 180°, but the corresponding equatorial angles $Fe_2$–$C_1$–$Fe_3$ and $Fe_4$–$C_1$–$Fe_5$ are distorted by equal magnitudes in opposite directions (+169.14° and −169.14° respectively), resulting in a 'ruffled' equatorial motif. In contrast, the crystal data for the *closo* core of $[Fe_6(\mu_6\text{-}C)(CO)_{16}]^{2-}$ show only small deviations from the ideal 180° for all three angles, with no clear pattern. However, the lengths of the Fe–Fe bonds in $\mathbf{2_{DFT}}$ deviate minimally from the Fe–Fe bond lengths in the crystallographically defined *closo* core of $[Fe_6(\mu_6\text{-}C)(CO)_{16}]^{2-}$ (Table 5).[32]

The four $\mu_2$-carbonyls in $\mathbf{2_{DFT}}$ are semi-bridging (as in the dianionic cluster) with asymmetric Fe–C bond lengths of 1.858 and 2.130 Å. Overall, the distortions from any PSEPT geometry (particular from *closo*) are reasonable for an electron deficient cluster in that no bonds are broken or drastically elongated. There is a slight (and expected) shortening of the metal–metal bonds and the metal–carbide bonds, with small changes in Fe–C–Fe bond angles to accommodate the strain. Meanwhile, the carbonyl bonding indicates no significant change compared with the 86 $e^-$ *closo* structure. Due to decreased electron density on the cluster (neutral *versus* $2^-$), a slight decrease in Fe–CO $\pi$ back-bonding leading to slightly longer Fe–CO and shorter C–O bonds was anticipated; however, this was not observed. We speculate that the change in Fe–CO bonding is limited due to the more significant distortions around the iron-carbide core. This phenomenon appears to compensate for the electron deficiency of the cluster.

Overall, the calculated structure of $\mathbf{2_{DFT}}$ exhibits limited distortions from the *closo* symmetry of the experimental structure of the corresponding dianion, albeit with slightly shortened iron-carbide bonds and a 'ruffling' of the equatorial iron-carbide bonds; the semi-bridging and terminal CO ligands remain relatively undisturbed. This suggests that the metastable, intermediate, non-PSEPT (14*n*) **2** accommodates the loss of two electrons from *closo* (14*n* + 2) primarily within the iron-carbide framework and Fe(CO) motifs with minimal overall changes.

**Vibrational analyses.** Provided the consistency of the computational vibrational spectra of $Fe_5(\mu_5\text{-}C)(CO)_{15}$ and $Fe_6(\mu_6\text{-}C)(CO)_{17}$ with experiment (see the ESI,† Computational methods), we performed the corresponding vibrational analysis of the intermediate cluster $\mathbf{2_{DFT}}$ with the same method. The calculated IR frequencies for $\mathbf{2_{DFT}}$ (intense features at 2018 and 1884 $cm^{-1}$) are reasonable for a neutral metal cluster with both terminal and semi-bridging carbonyl ligands. The experimental IR spectrum for **2** is limited in detail, exhibiting only a single broad feature in the $\nu$(C≡O) region at ~1990 $cm^{-1}$. The lack of resolution in the $\nu$(C≡O) region is attributed to the solution-drop-cast nature of the samples of reaction mixtures (see Table S1†, spectroscopic results section), rather than an isolated crystalline sample. Ultimately, the computational vibrational analysis for $\mathbf{2_{DFT}}$ provides a reasonable IR spectrum that is consistent with both its simulated structure and the experimental data.

Table 5 Selected bond distances (Å) and angles (°) of $[Fe_6(\mu_6\text{-}C)(CO)_{16}]$ ($\mathbf{2_{DFT}}$), $Fe_6(\mu_6\text{-}C)(CO)_{16}^{2-}$ (crystal data), and $Fe_6(\mu_6\text{-}C)(CO)_{18}$ (calculated)

| | $Fe_6(\mu_6\text{-}C)(CO)_{16}$ ($\mathbf{2_{DFT}}$) | $(PPh_4)_2[Fe_6(\mu_6\text{-}C)(CO)_{16}]^a$ | $Fe_6(\mu_6\text{-}C)(CO)_{18}{}^a$ (DFT) |
|---|---|---|---|
| PSEPT geometry | *Hypercloso* | *Closo* | *Nido* |
| axial $Fe_1$–$C_1$ | 1.880 | 1.878(5) | 2.0759 |
| axial $Fe_6$–$C_1$ | 1.880 | 1.874(5) | 2.0554 |
| $Fe_2$–$C_1$ | 1.894 | 1.886(5) | 1.9812 |
| $Fe_3$–$C_1$ | 1.894 | 1.898(5) | 1.9526 |
| $Fe_4$–$C_1$ | 1.894 | 1.897(4) | 1.8168 |
| $Fe_5$–$C_1$ | 1.894 | 1.881(4) | 1.8615 |
| $Fe_1$–$C_1$–$Fe_6$ | 180 | 174.51 | — |
| $Fe_2$–$C_1$–$Fe_4$ | 169.14 | 173.05 | — |
| $Fe_3$–$C_1$–$Fe_5$ | 169.14 | 177.62 | — |
| $Fe_1$–$Fe_2$ | 2.539 | 2.6561(9) | 2.4508 |
| $Fe_1$–$Fe_3$ | 2.792 | 2.5964(9) | 2.5963 |
| $Fe_1$–$Fe_4$ | 2.539 | 2.6771(9) | 2.9032 |
| $Fe_1$–$Fe_5$ | 2.792 | 2.7559(9) | 3.5890 |
| $Fe_2$–$Fe_3$ | 2.690 | 2.5795(8) | 2.8228 |
| $Fe_3$–$Fe_4$ | 2.690 | 2.8186(8) | 2.5851 |
| $Fe_4$–$Fe_5$ | 2.690 | 2.6663(8) | 2.6042 |
| $Fe_5$–$Fe_2$ | 2.690 | 2.6050(8) | 2.6730 |

[a] Ref. 32.

Table 6 Continuous shape measurement values for select $Fe_6C$ structure coordinates. Lower values indicate that the shape input is closer to the idealized polyhedra tested, which were $C_{5v}$ = pentagonal pyramid, $O_h$ = octahedron, and $D_{3h}$ = trigonal prism

| $Fe_6C$ structure | PSEPT class | $C_{5v}$ | $O_h$ | $D_{3h}$ |
|---|---|---|---|---|
| $Fe_6(\mu_6\text{-}C)(CO)_{18}$ | *nido* | 19.661 | 3.372 | 9.713 |
| $[Fe_6(\mu_6\text{-}C)(CO)_{16}]^{2-}$ | *closo* | 27.461 | 0.231 | 14.308 |
| $[Fe_6(\mu_6\text{-}C)(CO)_{16}]^{4-}$ | *closo* | 27.030 | 0.234 | 14.119 |
| $[Fe_6(\mu_6\text{-}C)(CO)_{16}]$ ($2_{GP\text{–}DFT}$) | *hypercloso* | 26.770 | 0.600 | 14.111 |
| $[Fe_6(\mu_6\text{-}C)(CO)_{17}]$ core A | *closo* | 28.978 | 0.087 | 15.653 |
| $[Fe_6(\mu_6\text{-}C)(CO)_{16}]$ core B | *closo* | 28.879 | 0.099 | 15.857 |

# Conclusions

We reach the following conclusions:

(1) The historical obstacle of performing ligand substitutions on the stable, canonical cluster $[Fe_6]^{2-}$ can be circumvented by redox-mediated ligand substitution. In particular, the *in situ* two-electron oxidation of $[Fe_6]^{2-}$ to $[Fe_6]^0$ provides an under-coordinated cluster that participates in simple ligand substitution reactions with phosphines. Evidence for the intact intermediate $[Fe_6]^0$ is supported spectroscopically and by the structurally characterized six-iron *closo* neutral cluster $Fe_6(\mu_6\text{-}C)(CO)_{17}$.

(2) The lack of ligand substitution for $[Fe_6]^{2-}$ is ascribed to both its fulfillment of PSEPT rules (86 $e^-$, *closo*) and its anionic charge. In contrast, ligand substitution is enabled in $[Fe_6]^0$ due to its non-PSEPT electron count (84 $e^-$, *pseudo–closo*) and neutral charge.

(3) The extent of phosphine substitution to the $[Fe_6]^0$ core between 1 and 3 ligated phosphines is determined by the σ donor strength of the applied phosphine, similar to the more synthetically challenging $[Fe_5]^0$.

(4) Intact iron-carbide clusters supported by the tripodal Triphos ligand can be isolated directly from the *in situ* oxidation of $[Fe_6]^{2-}$ (which, itself, can be synthesized on the gram-scale).

(5) The highlighted four-iron cluster $Fe_4(\mu_4\text{-}C)(\kappa_3\text{-}Triphos)(CO)_{10}$ retains the authentic carbide motif ($\mu_4$-C) and is the first authentic iron-carbide cluster chelated by an organic ligand framework.

(6) DFT analysis of the non-PSEPT $[Fe_6]^0$ cluster—*i.e.* the key reactive intermediate for ligand substitution—reveals that the $(\mu_6\text{-}C)Fe_6$ framework remains intact [*i.e.* no Fe–Fe, Fe–C or Fe–C(O) bonds are broken]. However, the structure becomes distorted into an axially compressed, ruffled octahedron rather than the tetragonally elongated octahedron of $[Fe_6]^{2-}$.

(7) DFT parameters (functional, % HF, basis set, and solvent continuum) were evaluated to model iron-carbide carbonyl clusters. The application of C-PCM implicit solvation improves the computational fidelity for anionic clusters, but decreases the structural accuracy of calculations on the corresponding neutral cluster models.

In closing, we highlight that the results herein demonstrate the validity of a general strategy of oxidative ligand addition to successfully install a designed donor set onto pre-existing iron-carbide carbonyl frameworks. We postulate that this approach presents a new opportunity for the facile synthesis of a range of new iron-carbide clusters. This represents a broader synthetic opportunity in nitrogenase-related, metal cluster chemistry.

# Data availability

All experimental data and detailed experimental procedures are available in the ESI† and the CCDC.

# Author contributions

Caitlyn R. Cobb: conceptualization, synthetic investigation, data curation, and manuscript preparation. Ren K. Ngo: computational investigation and validation. Emily J. Dick: synthetic investigation and data curation. Vincent M. Lynch: X-

ray diffraction data curation, formal analysis, and guidance on crystallographic analysis. Michael J. Rose: conceptualization, funding acquisition, project administration, and manuscript preparation.

## Conflicts of interest

There are no conflicts to declare.

## Acknowledgements

We thank the National Science Foundation (CHE-2109175) and Robert A. Welch Foundation (F-1822) for generous funding. CRC acknowledges an NSF-GRFP (DGE 2137420), and a University of Texas at Austin Provost Graduate Excellence Fellowship. EJD acknowledges a University of Texas at Austin, College of Natural Sciences Dean's Strategic Fellowship. We thank Dr Garrett Blake for assistance with the collection of $^{13}C$ and NOESY NMR data for the characterization of the interstitial carbide resonances. The authors acknowledge the Texas Advanced Computing Center (TACC) at The University of Texas at Austin for providing HPC resources that have contributed to the research results reported within this paper. URL: **http://www.tacc.utexas.edu**. We acknowledge the X-ray Diffraction Lab at the University of Texas at Austin for access to instrumentation.

## Notes and references

‡ This excludes the methylidyne cluster $Fe_4(\mu_4\text{-}\eta_2\text{-}CH)(CO)_{11}(PPh_3)$, as it is not an authentic $C^{4-}$ carbide.[22]

1 E. H. Braye, L. F. Dahl, W. Hübel and D. L. Wampler, *J. Am. Chem. Soc.*, 1962, **84**(24), 4633–4639, DOI: **10.1021/ja00883a004**.
2 M. R. Churchill, J. Wormald, J. Knight and M. J. Mays, *J. Am. Chem. Soc.*, 1971, **93**(12), 3073–3074, DOI: **10.1021/ja00741a058**.
3 M. R. Churchill and J. Wormald, *J. Chem. Soc., Dalton Trans.*, 1974, (22), 2410–2415, DOI: **10.1039/DT9740002410**.
4 M. A. Beno, J. M. Williams, M. Tachikawa and E. L. Muetterties, *J. Am. Chem. Soc.*, 1980, **102**(13), 4542–4544, DOI: **10.1021/ja00533a052**.
5 M. Tachikawa and E. L. Muetterties, *J. Am. Chem. Soc.*, 1980, **102**(13), 4541–4542, DOI: **10.1021/ja00533a051**.
6 A. D. Nguyen, M. D. Rail, M. Shanmugam, J. C. Fettinger and L. A. Berben, *Inorg. Chem.*, 2013, **52**(21), 12847–12854, DOI: **10.1021/ic4023882**.
7 N. D. Loewen, T. V. Neelakantan and L. A. Berben, *Acc. Chem. Res.*, 2017, **50**(9), 2362–2370, DOI: **10.1021/acs.accounts.7b00302**.
8 C. Cesari, J.-H. Shon, S. Zacchini and L. A. Berben, *Chem. Soc. Rev.*, 2021, **50**(17), 9503–9539, DOI: **10.1039/d1cs00161b**.
9 S. Pattanayak, N. D. Loewen and L. A. Berben, *Inorg. Chem.*, 2023, **62**(5), 1919–1925, DOI: **10.1021/acs.inorgchem.2c01556**.
10 N. S. Sickerman, K. Tanifuji, Y. Hu and M. W. Ribbe, *Chem.–Eur. J.*, 2017, **23**(51), 12425–12432, DOI: **10.1002/chem.201702496**.
11 L. Liu, T. B. Rauchfuss and T. J. Woods, *Inorg. Chem.*, 2019, **58**(13), 8271–8274, DOI: **10.1021/acs.inorgchem.9b01231**.
12 L. Liu, T. J. Woods and T. B. Rauchfuss, *Eur. J. Inorg. Chem.*, 2020, **2020**(36), 3460–3465, DOI: **10.1002/ejic.202000736**.
13 C. Joseph, C. R. Cobb and M. J. Rose, *Angew. Chem., Int. Ed.*, 2021, **60**(7), 3433–3437, DOI: **10.1002/anie.202011517**.
14 C. Joseph, J. P. Shupp, C. R. Cobb and M. J. Rose, *Catalysts*, 2020, **10**(11), 1317, DOI: **10.3390/catal10111317**.
15 P. L. Bogdan, M. Sabat, S. A. Sunshine, C. Woodcock and D. F. Shriver, *Inorg. Chem.*, 1988, **27**(11), 1904–1910, DOI: **10.1021/ic00284a018**.
16 A. Gourdon and Y. Jeannin, *Organometallics*, 1986, **5**(12), 2406–2410, DOI: **10.1021/om00143a002**.
17 M. J. Drance, C. C. Mokhtarzadeh, M. Melaimi, D. W. Agnew, C. E. Moore, A. L. Rheingold and J. S. Figueroa, *Angew. Chem., Int. Ed.*, 2018, **57**(40), 13057–13061, DOI: **10.1002/anie.201801206**.
18 J. S. Bradley, G. B. Ansell, M. E. Leonowicz and E. W. Hill, *J. Am. Chem. Soc.*, 1981, **103**(16), 4968–4970, DOI: **10.1021/ja00406a062**.
19 C. G. Cooke and M. J. Mays, *J. Organomet. Chem.*, 1975, **88**, 231–236, DOI: **10.1016/S0022-328X(00)91465-7**.
20 A. Gourdon and Y. Jeannin, *J. Organomet. Chem.*, 1990, **388**, 195–202, DOI: **10.1016/0022-328X(90)85362-3**.
21 J. S. Bradley, *Philos. Trans. R. Soc., A*, 1982, **308**, 103–113, DOI: **10.1098/rsta.1982.0152**.
22 H. Wadepohl, D. Braga and F. Grepioni, *Organometallics*, 1995, **14**(1), 24–33, DOI: **10.1021/om00001a009**.
23 J. H. Davis, M. A. Beno, J. M. Williams, J. Zimmie, M. Tachikawa and E. L. Muetterties, *Proc. Natl. Acad. Sci. U. S. A.*, 1981, **78**, 668–671, DOI: **10.1073/pnas.78.2.668**.
24 T. D. P. Stack and R. H. Holm, *J. Am. Chem. Soc.*, 1987, **109**(8), 2546–2547, DOI: **10.1021/ja00242a067**.
25 T. D. P. Stack and R. H. Holm, *J. Am. Chem. Soc.*, 1988, **110**(8), 2484–2494, DOI: **10.1021/ja00216a023**.
26 D. V. Fomitchev, C. C. McLauchlan and R. H. Holm, *Inorg. Chem.*, 2002, **41**(4), 958–966, DOI: **10.1021/ic011106d**.
27 A. McSkimming, A. Sridharan, N. B. Thompson, P. Müller and D. L. M. Suess, *J. Am. Chem. Soc.*, 2020, **142**(33), 14314–14323, DOI: **10.1021/jacs.0c06334**.
28 L. N. V. Le, G. A. Bailey, A. G. Scott and T. Agapie, *Proc. Natl. Acad. Sci. U. S. A.*, 2021, **118**(49), e2109241118, DOI: **10.1073/pnas.2109241118**.
29 L. N. V. Le, J. P. Joyce, P. H. Oyala, S. DeBeer and T. Agapie, *J. Am. Chem. Soc.*, 2024, **146**(8), 5045–5050, DOI: **10.1021/jacs.3c12025**.
30 A. G. Scott and T. Agapie, *J. Am. Chem. Soc.*, 2023, **145**(1), 2–6, DOI: **10.1021/jacs.2c04826**.
31 A. L. Nagelski, M. S. Fataftah, M. M. Bollmeyer, S. F. McWilliams, S. N. MacMillan, B. Q. Mercado, K. M. Lancaster and P. L. Holland, *Chem. Sci.*, 2020, **11**(47), 12710–12720, DOI: **10.1039/D0SC03447A**.

32 S. Kuppuswamy, J. D. Wofford, C. Joseph, Z.-L. Xie, A. K. Ali, V. M. Lynch, P. A. Lindahl and M. J. Rose, *Inorg. Chem.*, 2017, **56**(13), 5998–6012, DOI: 10.1021/acs.inorgchem.7b00741.
33 M. Bortoluzzi, I. Ciabatti, C. Cesari, C. Femoni, M. C. Iapalucci and S. Zacchini, *Eur. J. Inorg. Chem.*, 2017, **2017**(25), 3135–3143, DOI: 10.1002/ejic.201700169.
34 B. F. G. Johnson, R. D. Jonston and J. Lewis, *Chem. Commun. (London)*, 1967, (20), 1057a–1057a, DOI: 10.1039/c1967001057a.
35 J. Rimmelin, P. Lemoine, M. Gross, R. Mathieu and D. de Montauzon, *J. Organomet. Chem.*, 1986, **309**(3), 355–362, DOI: 10.1016/S0022-328X(00)99637-2.
36 J. R. Sowa Jr, V. Zanotti, G. Facchin and R. J. Angelici, *J. Am. Chem. Soc.*, 1991, **113**(24), 9185–9192, DOI: 10.1021/ja00024a026.
37 J. Evans, B. P. Gracey, L. R. Gray and M. Webster, *J. Organomet. Chem.*, 1982, **240**, C61–C64, DOI: 10.1016/S0022-328X(00)85149-9.
38 S. Ching, M. Sabat and D. F. Shriver, *J. Am. Chem. Soc.*, 1987, **109**(15), 4722–4723, DOI: 10.1021/ja00249a046.
39 B. F. G. Johnson, J. Lewis, J. N. Nicholls, J. Puga, P. R. Raithby, M. J. Rosales, M. McPartlin and W. Clegg, *J. Chem. Soc., Dalton Trans.*, 1983, 277–290, DOI: 10.1039/DT9830000277.
40 B. Berti, M. Bortoluzzi, C. Cesari, C. Femoni, M. C. Iapalucci, R. Mazzoni, F. Vacca and S. Zacchini, *Inorg. Chem.*, 2020, **59**(4), 2228–2240, DOI: 10.1021/acs.inorgchem.9b02912.
41 J. E. Barclay, A. Hills, D. L. Hughes and G. J. Leigh, *J. Chem. Soc., Dalton Trans.*, 1988, 2871–2877, DOI: 10.1039/DT9880002871.
42 N. D. Loewen and L. A. Berben, *Inorg. Chem.*, 2019, **58**, 16849–16857, DOI: 10.1021/acs.inorgchem.9b03102.
43 A. Gourdon and Y. Jeannin, *J. Organomet. Chem.*, 1992, **440**(3), 353–366, DOI: 10.1016/0022-328X(92)80214-I.
44 D. M. Norton, C. L. Stern and D. F. Shriver, *Inorg. Chem.*, 1994, **33**(13), 2701–2702, DOI: 10.1021/ic00091a001.
45 M. Akita, A. Sakurai and Y. Moro-oka, *Chem. Commun.*, 1999, 101–102, DOI: 10.1039/a808712a.
46 M. I. Bruce, B. D. Kelly, B. W. Skelton and A. H. White, *J. Organomet. Chem.*, 2000, **604**, 150–156, DOI: 10.1016/S0022-328X(00)00191-1.
47 M. I. Bruce, M. L. Cole, B. G. Ellis, M. Gaudio, B. K. Nicholson, C. R. Parker, B. W. Skelton and A. H. White, *Polyhedron*, 2015, **86**, 43–56, DOI: 10.1016/j.poly.2014.04.052.
48 M. I. Bruce, M. L. Cole, C. R. Parker, B. W. Skelton and A. H. White, *Organometallics*, 2008, **27**(14), 3352–3367, DOI: 10.1021/om7010968.
49 W.-K. Wong, K. W. Chiu, G. Wilkinson, A. M. R. Galas, M. Thornton-Pett and M. B. Hursthouse, *J. Chem. Soc., Dalton Trans.*, 1983, 1557–1563, DOI: 10.1039/DT9830001557.
50 C. C. Lu, C. T. Saouma, M. W. Day and J. C. Peters, *J. Am. Chem. Soc.*, 2007, **129**(1), 4–5, DOI: 10.1021/ja065524z.
51 C. T. Saouma, C. C. Lu and J. C. Peters, *Inorg. Chem.*, 2012, **51**(18), 10043–10054, DOI: 10.1021/ic301704f.
52 M. Kaupp, *Chem. Commun.*, 1996, 1141–1142, DOI: 10.1039/cc9960001141.
53 J. McGale, G. E. Cutsail III, C. Joseph, M. J. Rose and S. Debeer, *Inorg. Chem.*, 2019, **58**(19), 12918–12932, DOI: 10.1021/acs.inorgchem.9b01870.
54 K. A. Moltved and K. P. Kepp, *J. Chem. Theory Comput.*, 2018, **14**(7), 3479–3492, DOI: 10.1021/acs.jctc.8b00143.
55 M. U. Delgado-Jaime, B. R. Dible, K. P. Chiang, W. W. Brennessel, U. Bergmann, P. L. Holland and S. DeBeer, *Inorg. Chem.*, 2011, **50**(21), 10709–10717, DOI: 10.1021/ic201173j.
56 M. Cossi, N. Rega, G. Scalmani and V. Barone, *J. Comput. Chem.*, 2003, **24**(6), 669–681, DOI: 10.1002/jcc.10189.
57 V. Barone and M. Cossi, *J. Phys. Chem. A*, 1998, **102**, 1995–2001, DOI: 10.1021/jp9716997.
58 D. M. P. Mingos and D. J. Wales, *Introduction to Cluster Chemistry*, Prentice-Hall Inc, Englewood Cliffs, New Jersey, 1st edn, 1990.
59 R. L. Johnston and D. M. P. Mingos, *Inorg. Chem.*, 1986, **25**(18), 3321–3323, DOI: 10.1021/ic00238a043.
60 M. L. McKee, Z.-X. Wang and P. von Ragué Schleyer, *J. Am. Chem. Soc.*, 2000, **122**(19), 4781–4793, DOI: 10.1021/ja994490a.
61 W. Mesbah, M. Soleimani, E. Kianfar, G. Geiseler, W. Massa, M. Hofmann and A. Berndt, *Eur. J. Inorg. Chem.*, 2009, **2009**(26), 5577–5582, DOI: 10.1002/ejic.200900850.
62 S. J. Bonyhady, D. Collis, N. Holzmann, A. J. Edwards, R. O. Piltz, G. Frenking, A. Stasch and C. Jones, *Nat. Commun.*, 2018, **9**, DOI: 10.1038/s41467-018-05504-x.
63 R. T. Baker, *Inorg. Chem.*, 1986, **25**(1), 109–111, DOI: 10.1021/ic00221a029.
64 J. D. Kennedy, *Inorg. Chem.*, 1986, **25**(1), 111–112, DOI: 10.1021/ic00221a030.
65 M. Pinsky and D. Avnir, *Inorg. Chem.*, 1998, **37**(21), 5575–5582, DOI: 10.1021/ic9804925.